Chinese Journal of Natural Medicines

Deciphering chemical and metabolite profiling of Chang-Kang-Fang by UPLC-Q-TOF-MS/MS and its potential active components identification

Fengge YANG, Sihao ZHANG, Danmei TIAN, Guirong ZHOU, Xiyang TANG, Xinglong MIAO, Yi HE, Xinsheng YAO, Jinshan TANG

Citation: Fengge YANG, Sihao ZHANG, Danmei TIAN, Guirong ZHOU, Xiyang TANG, Xinglong MIAO, Yi HE, Xinsheng YAO, Jinshan TANG, Deciphering chemical and metabolite profiling of Chang-Kang-Fang by UPLC-Q-TOF-MS/MS and its potential active components identification, Chinese Journal of Natural Medicines, 2023, 21(6), 459-480. doi: 10.1016/S1875-5364(23)60474-1.

View online: https://doi.org/10.1016/S1875-5364(23)60474-1

Wechat

Available online at www.sciencedirect.com
ScienceDirect
Chinese Journal of Natural Medicines 2023, **21**(6): 459-480
doi: 10.1016/S1875-5364(23)60474-1
Chinese Journal of Natural Medicines

•Original article•

Deciphering chemical and metabolite profiling of Chang-Kang-Fang by UPLC-Q-TOF-MS/MS and its potential active components identification

YANG Fengge[1Δ], ZHANG Sihao[1Δ], TIAN Danmei[1Δ], ZHOU Guirong[2, 3], TANG Xiyang[1], MIAO Xinglong[2, 3], HE Yi[2, 3*], YAO Xinsheng[1*], TANG Jinshan[1*]

[1] *Institute of Traditional Chinese Medicine and Natural Products, College of Pharmacy/Guangdong Province Key Laboratory of Pharmacodynamic Constituents of Traditional Chinese Medicine and New Drug Research/International Cooperative Laboratory of Traditional Chinese Medicine Modernization and Innovative Drug Development of Ministry of Education (MOE) of China, Jinan University, Guangzhou 510632, China;*

[2] *State Key Laboratory of Core Technology in Innovative Chinese Medicine, Tasly Pharmaceutical Group Co., Ltd., Tianjin 300410, China;*

[3] *Tasly Pharmaceutical Group Co., Ltd., Tianjin 300410, China*

Available online 20 Jun., 2023

[ABSTRACT] Chang-Kang-Fang (CKF) formula, a Traditional Chinese Medicine (TCM) prescription, has been widely used for the treatment of irritable bowel syndrome (IBS). However, its potential material basis and underlying mechanism remain elusive. Therefore, this study employed an integrated approach that combined ultra-performance liquid chromatography-quadrupole time-of-flight mass spectrometry (UPLC-Q/TOF-MS) with network pharmacology to systematically characterize the phytochemical components and metabolites of CKF, as well as elucidating its underlying mechanism. Through this comprehensive analysis, a total of 150 components were identified or tentatively characterized within the CKF formula. Notably, six *N*-acetyldopamine oligomers from *Cicadae Periostracum* and eight resin glycosides from *Cuscutae Semen* were characterized in this formula for the first time. Meanwhile, 149 xenobiotics (58 prototypes and 91 metabolites) were detected in plasma, urine, feces, brain, and intestinal contents, and the *in vivo* metabolic pathways of resin glycosides were elaborated for the first time. Furthermore, network pharmacology and molecular docking analyses revealed that alkaloids, flavonoids, chromones, monoterpenes, *N*-acetyldopamine dimers, *p*-hydroxycinnamic acid, and Cus-3/isomer might be responsible for the beneficial effects of CKF in treating IBS, and CASP8, MARK14, PIK3C, PIK3R1, TLR4, and TNF may be its potential targets. These discoveries offer a comprehensive understanding of the potential material basis and clarify the underlying mechanism of the CKF formula in treating IBS, facilitating the broader application of CKF in the field of medicine.

[KEY WORDS] Chang-Kang-Fang; Chemical profile; Metabolites profile; UPLC-Q-TOF/MS; Network pharmacology; Molecular docking

[CLC Number] R91 **[Document code]** A **[Article ID]** 2095-6975(2023)06-0459-22

Introduction

Irritable bowel syndrome (IBS) is a functional disorder of the gastrointestinal tract with a global prevalence of 10%−15%. Its cardinal symptoms encompass chronic or recurrent abdominal pain, diarrhea, and altered bowel habits [1]. Despite extensive research, the precise etiological factors contributing to IBS remain elusive. However, it is widely acknowledged that the condition is multifactorial in nature, involving various mechanisms such as altered intestinal permeability, disturbances in brain-gut interactions, inflammation, and visceral hypersensitivity [2-4]. Conventional medical treatments for IBS, such as loperamide, eluxadoline, and trimebutine maleate, primarily target specific symptoms or pathways, resulting in moderate therapeutic outcomes [5].

Traditional Chinese Medicine (TCM) prescriptions, characterized by their multi-component nature and multi-target effects, have gained considerable attention as potential therapeutic approaches for complex diseases. One such prescrip-

[Received on] 02-Nov.-2022
[Research funding] This research was supported by National Key Research and Development Program of China (No. 2017ZX 09301005).
[*Corresponding author] E-mails: heyi@tasly.com (HE Yi); tyaoxs@jnu.edu.cn (YAO Xinsheng); gztangjinshan@126.com (TANG Jinshan)
[Δ]These authors contributed equally to this work.
These authors have no conflict of interest to declare.

tion is the Chang-Kang-Fang (CKF) formula, derived from the classical TCM prescriptions "Tongxie Yaofang" and "Xinshen Wan" documented in the TCM classic *Jing Yue Quan Shu*. Composed of seven medical herbs, including Paeoniae Radix Alba (PRA), Saposhnikoviae Radix (SR), Coptidis Rhizoma (CR), Cuscutae Semen (CS), Rehmanniae Radix Praeparata (RRP), Fagopyri Dibotryis Rhizoma (FDR), and Cicadae Periostracum (CP), the CKF formula has exhibited notable clinical efficacy in the treatment of IBS. In fact, its effectiveness in alleviating IBS symptoms, such as diarrhea and abdominal pain, has been demonstrated to be comparable to or even surpassing that of trimebutine maleate, a clinical first-line medication, with an effective rate of 85.2% [6]. Recent pharmacological studies have revealed that the CKF formula can modulate the brain-gut axis by promoting the production of calcitonin gene-related peptide (CGRP), vasoactive intestinal peptide (VIP), 5-HT, and substance P (SP), thereby exerting its therapeutic effects in IBS treatment. Furthermore, CKF has also shown the capacity to regulate gut microbiota [7, 8]. However, the specific active ingredients responsible for the favorable effects of CKF and the underlying mechanism remain to be elucidated.

Given the potential role of the constituents in TCM prescriptions, particularly the prototypes and their *in vivo* metabolites, in mediating therapeutic efficacy, a comprehensive understanding of the chemical and metabolic profiles of CKF extracts is of paramount importance for elucidating its underlying mechanisms and facilitating clinical applications. Although many studies have investigated the chemical components and metabolic behaviors of individual herbal medicines within the CKF formula, only one report has provided insights into the chemical profile of the CKF formula [8]. However, this previous investigation failed to identify any components from CP, and only two components were characterized from FDR in the CKF extracts. Additionally, no study has explored the *in vivo* metabolic profile and pathways associated with the administration of the CKF formula.

This study employed an integrated approach combining *in vitro* chemical profiling and *in vivo* metabolic analysis of CKF extracts in rats, utilizing ultra-performance liquid chromatography-quadrupole time-of-flight mass spectrometry (UPLC-Q/TOF-MS) coupled with network pharmacology-based signaling pathway enrichment. The aim was to determine the potential active components of the CKF formula for treating IBS and to clarify its underlying mechanism. This study encompassed three main aspects: (1) systemic characterization of the holistic chemical composition of CKF extracts, laying a foundation for further *in vivo* metabolic investigations; (2) characterization of the absorption and metabolic profiles of CKF extracts *in vivo* to identify potential active components; (3) identification of potentially active components and their associated mechanisms using network pharmacology and molecular docking analyses. It is anticipated that the findings of this study will contribute to a better understanding of the pharmacodynamic mechanisms underlying the CKF formula and facilitate subsequent quality control measures for its clinical application (Fig. 1).

Materials and Methods

Materials and reagents

The Chang-Kang-Fang extract (Lot No. 20201201) was provided by Tasly Pharmaceutical Group Co., Ltd. (Tianjin, China). Epiberberine, epicatechin, hyperoside, quercetin, kaempferol, jatrorrhizine, leonuride, isoquercitrin, palmatine, berberine, coptisine, paeoniflorin, 5-*O*-methylvisammioside, (+)-catechin, and astragalin were purchased from Shanghai Yuanye Bio-Technology Co., Ltd. (Shanghai, China). Albiflorin, cimifugin, prim-*O*-glucosylcimifugin, and catalpol were purchased from Shanghai Acmec Biochemical Co., Ltd. (Shanghai, China). Oxypaeoniflorin and sec-*O*-glucosylhamaudol were purchased from Chengdu Push Bio-technology Co., Ltd. (Chengdu, China). Echinacoside and benzoylpaeoniflorin were purchased from Shanghai Macklin Biochemical Co., Ltd. (Shanghai, China). Each reference compound exhibited a purity exceeding 98%, as determined by High-performance liquid chromatography (HPLC) analysis. Acetonitrile, methanol, and water of liquid chromatography-mass spectrometry (LC-MS) grade were obtained from Fisher Scientific (Fair Lawn, New Jersey, USA), and formic acid of LC-MS grade was acquired from Sigma-Aldrich (St. Louis, USA). All other reagents used were of analytical grade.

Reference standards and CKF sample preparation

A precise amount of Chang-Kang-Fang (CKF) extract weighing 20 mg was meticulously measured and suspended in 1 mL of methanol/water solution (7 : 3, *V/V*) in an ultrasonic water bath for 10 min. After that, the resulting sample solution was centrifuged at 13 000 r·min^{-1} for 10 min, and 2 μL of the supernatant aliquot was extracted for UPLC-Q/TOF-MS analysis. To qualitatively identify the components of CKF, all reference standards were individually dissolved in methanol, blended at specific ratios, and stored at 4 °C until analysis. For drug administration, the CKF extract was suspended in water to obtain the normal- and high-dose groups with concentrations of 0.05 and 0.25 g·mL^{-1}, respectively.

Animals and drug administration

Ten male Sprague-Dawley (SD) rats weighing approximately 250 g were purchased from the Experimental Animal Center of Guangdong Province (Guangzhou, China). Prior to the experiment, the rats underwent a 12-day acclimation period, during which they were provided with ad libitum access to a standard laboratory diet and water. They were housed under controlled conditions with an ambient temperature of 23 ± 2 °C and a twelve-hour light/dark cycle. Subsequently, the rats were individually placed in metabolic cages overnight, allowing free access to water in preparation for the experiment. Ethical clearance for the animal study was obtained from the Institutional Animal Care and Use Committee (IACUC) of Jinan University (Approval No. IACUC-20210830-24). All experimental procedures adhered to guidelines outlined in the *Guide for the Care and Use of Laboratory Animals* (National Institutes of Health). The ten rats were randomly divided into three groups, namely the CKF high-dose group (n = 4), CKF normal-dose group (n = 4), and blank group (n = 2). The CKF extract suspension was

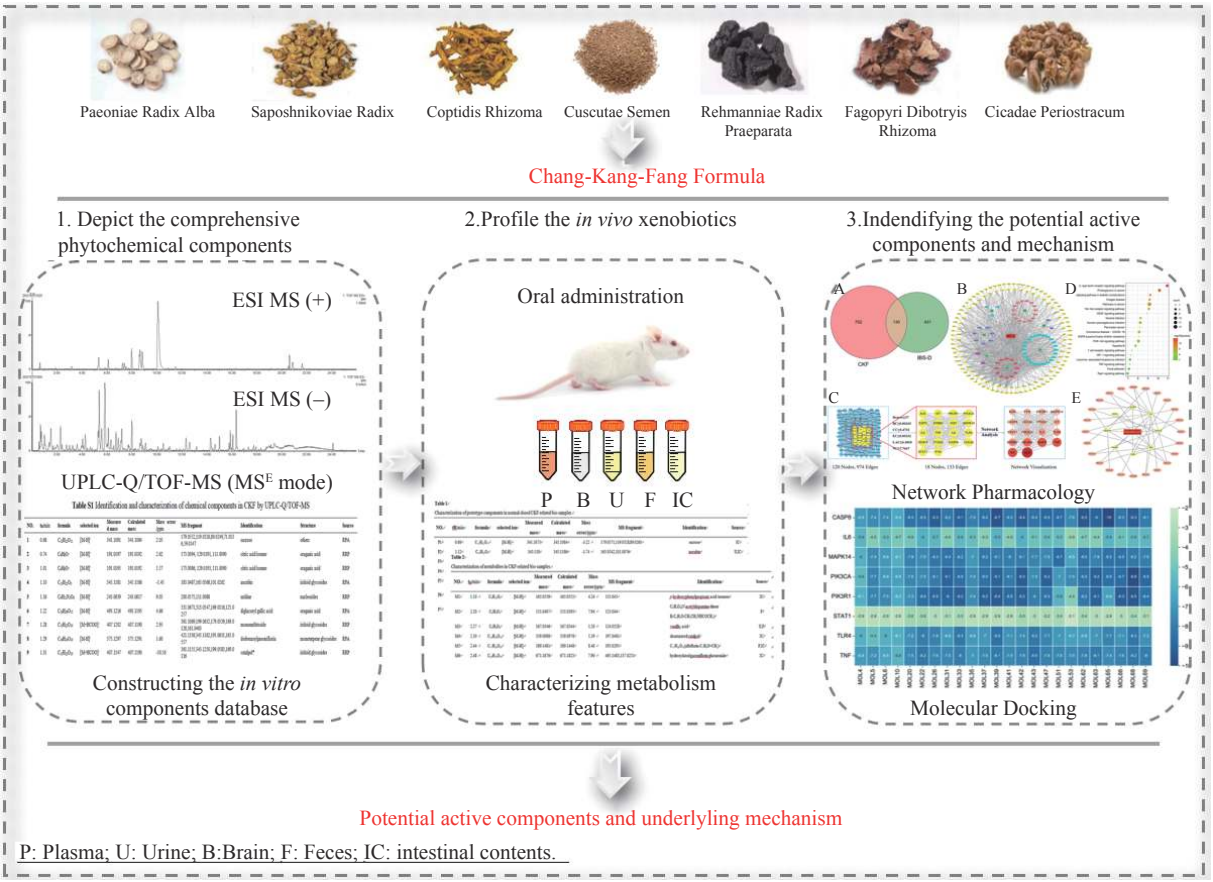

Fig. 1 Systematic investigation strategy of this research.

administered *via* the intragastric route to the high- and normal-dose groups at dosages of 3.01 g·kg^{-1}·day^{-1} (five times the normal dosage) and 0.60 g·kg^{-1}·day^{-1} (equivalent to the dosage of CKF granules employed in clinical studies), respectively, for three days. In the meantime, the blank group was given drinking water using the same administration method.

Bio-sample collection and pretreatment

Plasma samples

Rats in the drug administration groups were anesthetized, and hepatic portal vein blood samples were collected at designated time points (0.5 h, 1 h, 2 h, and 4 h) after the final administration. A single rat was utilized for each time point, and the blood samples were collected into separate heparinized tubes. In parallel, plasma samples were collected from the blank group following the last water administration. Subsequently, the plasma samples were centrifugated at 13 000 r·min^{-1} for 10 min at 4 °C to achieve protein precipitation. For this purpose, 1 mL aliquots of plasma were mixed with 3 mL of acetonitrile, followed by vortex mixing and centrifugation at 14 000 r·min^{-1} for 10 min. The resulting supernatant was then dried under nitrogen gas at room temperature and dissolved in 200 μL of methanol before UPLC-Q/TOF-MS detection.

Urine and feces samples

Urine and feces samples were collected over a period of 48 h following the initial administration. Urine samples were pooled within their respective groups and subjected to centrifugation at 9960 r·min^{-1} for 10 min. Then the resulting supernatant was loaded onto the pre-treated HLB columns (3 cc, 60 mg, Waters Oasis) and eluted with 6 mL of 5% methanol/water (*V*/*V*) and 6 mL of methanol. The eluted methanol fraction was collected and dried under nitrogen gas, yielding a urine sample residue, which was dissolved in 1 mL of methanol for subsequent UPLC/Q-TOF-MS analysis. For feces samples, 1 g of dried feces from each group was pulverized to a powder and then subjected to ultrasonic extraction with 10 mL of methanol for 60 min. The resulting mixture was centrifuged at 9960 r·min^{-1} for 10 min, and the supernatant was collected. After drying under nitrogen gas, the residue was suspended in 5 mL of deionized water and loaded onto pre-activated HLB columns for purification. The methanol fraction was collected using the same procedure as the urine samples. Finally, the residue was obtained after drying under nitrogen gas and dissolved in 1 mL of methanol before UPLC/Q-TOF-MS analysis.

Brain samples

After the collection of plasma samples, the brains of the experimental animals were immediately dissected and washed with a cold saline solution. The brain tissues were then homogenized using a saline solution at a ratio of 4 : 1 (volume). A portion of the homogenized brain sample (2 mL) from each group was mixed with 8 mL of acetonitrile and

subjected to vortex mixing for 3 min to facilitate protein precipitation. The resulting supernatant was obtained by centrifugation at 14 000 r·min^{-1} for 10 min and dried under nitrogen gas at room temperature. The resulting residue was dissolved in 200 μL of methanol prior to UPLC/Q-TOF-MS analysis.

Intestinal content samples

After the hepatic portal vein blood collection, the intestinal tissues with their luminal contents were promptly procured. Subsequently, the luminal contents of the intestines were thoroughly flushed out utilizing a saline solution. The collected intestinal content samples were subjected to lyophilization, followed by pulverization into a fine powder. Precise measurements of 0.1 g of the intestinal content samples from each experimental group were performed, and these samples were then meticulously suspended in 1 mL of methanol. Following a vortex mixing for 3 min, the samples were extracted in an ultrasonic ice-water bath for 30 min. The resulting supernatant was obtained by subjecting the samples to additional vortex mixing and subsequent centrifugation at 14 000 r·min^{-1} for 10 min. Finally, the samples were dried under nitrogen gas at room temperature, and the residue was dissolved in 200 μL of methanol in preparation for UPLC/Q-TOF-MS analysis.

UPLC-Q/TOF-MS analysis

UPLC analysis was performed on an ACQUITY^{TM} UPLC I-Class system equipped with a binary solvent system and an automated sample manager. The chromatographic separation was achieved on an Acquity UPLC BEH C_{18} Column (2.1 mm × 100 mm, 1.7 μm) with the following mobile phases: eluent A (0.1 % formic acid in water, *V*/*V*) and eluent B (0.1 % formic acid in acetonitrile, *V*/*V*). A linear gradient program was employed as follows: 2%–10% B (0–3 min); 10%–20% B (3–7 min); 20%–30% B (7–12 min); 30%–35% B (12–14 min); 35%–50% B (14–17 min); 50%–100% B (17–20 min); 100% B (20–23 min); 2% B (23–24.5 min); 2% B (24.5–26 min). The flow rate was maintained at 0.4 mL·min^{-1}, and the injection volume for analysis was 2 μL.

The UPLC system was coupled to a SYNAPTTM G2 HDMS Q-TOF tandem mass spectrometer with an electrospray ionization (ESI) source (Waters, Manchester, UK). The ESI source was operated at a capillary voltage of 3 kV for positive ion mode and −2.5 kV for negative ion mode. The sample cone voltage was set at 35 V in positive mode and 40 V in negative mode. The source temperature was maintained at 100 °C, while the desolvation temperature was set to 300 °C. The cone gas flow and desolvation gas flow were set at 50 L·h^{-1} and 800 L·h^{-1}, respectively. During data acquisition, the MS^{E} mode was utilized, with a low-energy function trap collision energy set to 5 eV and a high-energy function ramp trap collision energy ranging from 20 to 50 eV. Collision-induced dissociation (CID) experiments were carried out using argon as the collision gas. The mass spectrometer was calibrated across a range of 50–1500 Da using a sodium formate solution to ensure mass accuracy and reproducibility. For lock mass correction, leucine-enkephalin was employed as an external reference compound and infused at a constant flow of 5 L·min^{-1} using LockSpray^{TM} mode. In positive ion mode, the lock mass value was set to *m/z* 556.2771, while in negative ion mode, it was set to *m/z* 554.2615. The acquired data were recorded in centroid mode. Subsequent data analysis was performed using Masslynx software (V4.1, Waters, Milford, MA, USA) to extract meaningful information from the spectra obtained in both positive and negative ion modes.

Network pharmacology analysis

The canonical Simplified Molecular-Input Line-Entry System (SMILES) representations of 69 candidate compounds were generated using ChemDraw 20.0 software. These SMILES representations were then inputted into Similarity Ensemble Approach (SEA) database (http://sea.bkslab.org/) and SwissTargetPrediction database (http://www.swisstargetprediction.ch/) for target prediction. To identify IBS-related targets, we conducted searches using keywords, "diarrhea predominant" "irritable bowel syndrome" in the DisGeNET (https://www.disgenet.org/) and GenCards database (https://www.genecards.org/). The overlapping genes between the targets predicted for the candidate compounds and the disease-related targets were determined using Venny 2.1 software (https://bioinfogp.cnb.csic.es/tools/venny/), and the protein-protein interaction (PPI) data were obtained from the String database (V11.0, https://cn.string-db.org/). The resulting PPI network was visualized using Cytoscape 3.9.0, and key targets were identified based on parameters including betweenness centrality (BC), closeness centrality (CC), eigenvector centrality (EC), local average connectivity (LAC), and network centrality (NC). The Kyoto Encyclopedia of Genes and Genomes (KEGG) enrichment pathway analysis of significant targets was performed on the Database for Annotation, Visualization, and Integrated Discovery (DAVID, V6.8, http://david.ncifcrf.gov) to predict potential signaling pathways involved in CKF against IBS. Ultimately, potential targets and pathways, together with their corresponding active ingredients of CKF for the treatment of IBS, were identified, and the results were plotted using the Bioinformatics Web Server (http://www.bioinformatics.com.cn).

Molecular docking verification

To validate the network pharmacology results, we performed molecular docking to investigate the interaction pattern between potential targets and 24 prototype compounds. Firstly, the crystallographic structures of receptor proteins were obtained from Protein Data Bank (http://www.rcsb.org). Concurrently, the molecular structures of the prototypes were optimized to their minimum energy conformation using Chem3D V20.0. Subsequently, the ligand molecules and receptor proteins were prepared and subjected to docking simulations using AutoDock Vina. The resulting docking scores were used to elucidate the binding pattern between potential targets and 24 prototype compounds. Finally, the results were visualized using PyMOL V2.3.4 and PLIP (https://plip-tool.biotec.tu-dresden.de/plip-web/plip/index).

Results

Data analysis strategy

To characterize the chemical components of the CKF

formula, we performed UPLC/Q-TOF-MS analysis in the MS^E mode. This involved the acquisition of data for reference standards, individual herbal components, and CKF extracts in both positive and negative ion modes. The obtained data allowed for the characterization of fragmentation patterns in the reference standards. By comparing accurate molecular weights, fragmentation pathways, and the retention time of peaks in the CKF extracts with those of reference standards and previous reports, the chemical components of the CKF extracts were identified and recorded in an *in vitro* component database (Table S1). Furthermore, the component assignment was confirmed by comparing the chromatograms of the CKF extracts with those of individual herbs. On the basis of the *in vitro* chemical profile investigation, a two-step strategy was applied to decipher the *in vivo* metabolic profile of the CKF extracts. Initially, a high dose of CKF extracts (3.01 $g \cdot kg^{-1} \cdot d^{-1}$, five times the normal dosage) was administered to SD rats to identify the xenobiotics in bio-samples using the *in vitro* component database and Metabolynx XS software (V4.1, Waters) (Table S2). The identification was confirmed by comparing characteristic fragments and neutral losses with those of reference standards and previous reports. Subsequently, the metabolic profile of the CKF extracts at the normal dosage (0.60 $g \cdot kg^{-1} \cdot d^{-1}$) was easily deciphered based on the findings from the high-dose administration.

Identification and characterization of chemical components in CKF

A qualitative analysis of chemical components in CKF extracts was conducted using UPLC/Q-TOF-MS. As a result, a total of 150 compounds were identified in the CKF extracts, including 20 alkaloids, 24 flavonoids, 23 phenolic acids, 8 chromones, 5 coumarins, 7 iridoid glycosides, 7 phenylpropanoid glycosides, 6 *N*-acetyldopamine oligomers, 33 monoterpenes, 8 resin glycosides, and 9 compounds of other types. Among these, 23 compounds were unambiguously identified by comparing their retention time and accurate molecular weights with those of the reference standards. The base peak intensity (BPI) chromatograms of the CKF extracts in positive and negative ion modes are shown in Fig. 2, and detailed information regarding their chemical components is listed in Table S1.

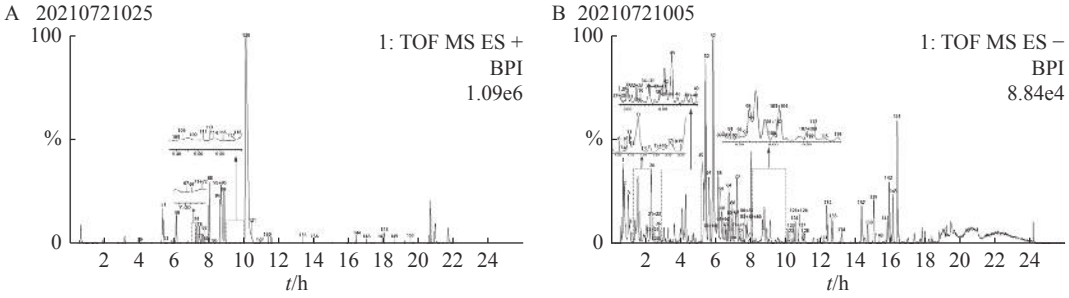

Fig. 2 BPI chromatograms of CKF extracts in positive (A) and negative (B) ion modes.

Identification of alkaloids in CKF

Alkaloids are prominent components in CR known for their biological function. In this study, 20 alkaloids were identified from CKF extracts, including 18 protoberberine alkaloids, 1 tetrahydroprotoberberine alkaloid, and 1 aporphine alkaloid. Among them, protoberberine and tetrahydroprotoberberine alkaloids share the same tetracyclic skeleton that is derived from a benzyltetrahydroisoquinoline system with the incorporation of an extra carbon atom, supplied from *S*-adenosylmethionine (SAM). Aporphine alkaloid is the product of an oxidative coupling of benzyltetrahydroisoquinoline [9].

Protoberberine alkaloids share a common core structure but differ in the substituents at C-2, C-3, C-9, C-10, and C-13, which can be differentiated by tandem mass spectrometry (MS/MS) experiments. For example, the presence of vicinal dimethoxy groups at C-9 and C-10 can be easily identified by the release of methyl and H radicals (CH_4), resulting in the formation of a 1,3-dioxypentacyclic ring, followed by the neutral loss of CO from the newly formed ring. In the CKF extracts, ten compounds (**67**, **79**, **90**, **94**, **99**, **114**, **120**, **121**, **129**, and **144**) had the same fragmentation pattern as mentioned above, indicative of protoberberine alkaloids with vicinal dimethoxy groups at C-9 and C-10. Compounds possessing a single methoxy group at either C-9 or C-10 tended to undergo the loss of a methyl radical (**72** and **78**). The diagnostic ion $[M - CO]^+$ is usually used to infer the presence of a methylenedioxy group at C-9 and C-10 but not at C-2 and C-3 due to the stability of methylenedioxy group at C-2 and C-3. Therefore, compounds **84**, **95**, **96**, **106**, **111**, and **116** in the CKF extracts possessed a methylenedioxy group at C-9 and C-10. The molecular weights and similar fragmentation patterns mentioned above facilitated the determination of substituents at other positions. In addition, compounds **95**, **96**, **99**, **120**, and **121** were unequivocally assigned as coptisine, epiberberine, jatrorrhizine, berberine, and palmatine, respectively, by comparison with reference standards.

Tetrahydroprotoberberine alkaloids exhibit a notable predilection for Retro Diels-Alder (RDA) cleavage at ring C, accompanied by the concomitant loss of side-chain substituents observed in the MS/MS spectrum. Consequently, compound **69** was assigned as *N*-methylcorydalmine. Aporphine alkaloids are susceptible to ring B opening, leading to the loss of the nitrogenous moiety, followed by the release of a methyl radical. For example, compound **51** ($C_{20}H_{24}NO_4$) was identified as magnoflorine [10], displaying characteristic ions at *m/z* 297.1126 $[M - (CH_3)_2NH]^+$ and 282.0898 $[M - (CH_3)_2NH) -$

$CH_3]^-$, corresponding to the cleavage of ring B.

Identification of flavonoids in CKF

Flavonols and their glycosides represent the characteristic components of CS, whereas flavanols are the distinctive components of FDR. In this study, 24 flavonoids were identified from CKF extracts, including 2 flavanols, 2 flavonols, and 20 flavonol glycosides.

Structurally, flavonols are derivatives of 2-phenylchromanone-3-ol and can be converted into flavanols by reducing the carbonyl of C-4 and double bonds at C-2 and C-3, thereby exhibiting discernible differences in the fragment ions resulting from Retro Diels-Alder (RDA) cleavage of ring C [11]. Specifically, flavanols **38** and **49** demonstrated distinctive fragment ions at *m/z* 137.02 $[C_7H_6O_3 - H]^-$, while flavonols **122** and **131** displayed characteristic fragment ions at *m/z* 151.00 $[C_7H_4O_4 - H]^-$, owing to the RDA cleavage. By comparison with authentic standards, compounds **38**, **49**, **122**, and **131** were accurately assigned as catechin, epicatechin, quercetin, and kaempferol, respectively.

Flavonol glycosides commonly exhibit sugar moieties attached to C-3, C-7, or both positions. Their fragmentation patterns involve successive losses of sugar units, such as glucose, rhamnose, and apiose. Subsequently, they undergo conversion into aglycones that can be classified as quercetin, kaempferol, or isorhamnetin, based on their core structures, with diagnostic ions observed at *m/z* 285.04, 301.03, and 315.05, respectively. In addition, the intensity of ions can be used to determine the position of sugar substitutions [12]. Specifically, the intensity of $[Aglycone - H]^-$ ion surpasses that of the $[Aglycone]^-$ ion when the sugar moiety is attached to C-3 rather than C-7, and vice versa. Furthermore, the diagnostic ion $[Aglycone - 2H]^-$ could be observed when two sugar chains existed in different positions [11]. Based on rules mentioned above and comparative analysis with previous studies [11-12], compounds **41**, **43**, and **68** were identified as flavonol glycosides with dual sugar chains at C-3 and C-7; compounds **87**, **102**, and **125** were tentatively characterized to be flavonol glycosides with one sugar chain at C-7; while compounds **47**, **60**, **61**, **63-65**, **75**, **77**, **83**, **85**, **103**, **108**, **115**, and **123** were tentatively assigned as flavonol glycosides with a single sugar chain at C-3. Notably, compounds **64**, **65**, and **83** were unambiguously identified as hyperoside, isoquercitrin, and astragalin, respectively, through comparison with reference standards.

Identification of phenolic acids in CKF

In the present study, the comprehensive profiling of phenolic acids in CKF extracts yielded the identification of 23 distinct compounds. Among these, ten were classified as chlorogenic acids, six as gallic acids, and the remaining seven as other phenolic acids. The primary botanical sources of these compounds were CS, FDR, CR, CP, and PRA. Their MS/MS spectra exhibited characteristic fragmentation patterns characterized by neutral losses of H_2O, CO, and CO_2.

Chlorogenic acids, mainly derived from CS, are esterification products of quinic acid, usually in conjunction with cinnamic acids. If cinnamic acids were substituted with glycosyl units, the initial loss of sugar units is observed. For example, compounds **22**, **26**, and **32** display a characteristic neutral loss of $C_6H_{10}O_5$ (sugar unit) in their MS/MS spectra, indicating the presence of glucose. Subsequently, they exhibit a tendency to lose cinnamic acids such as caffeoyl and feruloyl, resulting in the production of diagnostic ions at *m/z* 191.05 $[quinic\ acid - H]^-$, 173.04 $[quinic\ acid - H - H_2O]^-$, 179.03 $[caffeic\ acid - H]^-$, and 193.05 $[ferulic\ acid - H]^-$. The intensity of diagnostic ions could be used to determine the site of esterification. The base peak, for example, at *m/z* 191.05 signifies esterification at 3-OH or 5-OH, and the peak at *m/z* 173.04 indicates esterification at 4-OH [12]. Compounds **27**, **30**, and **44** had the same molecular formula of $C_{16}H_{18}O_9$, and all displayed diagnostic ions at *m/z* 191.05, 179.03, and 173.04 in the MS/MS spectra, indicating that they are derivatives of caffeoylquinic acids. Previous studies have revealed a more pronounced ion at *m/z* 179.03 when caffeic acid is linked to 3-OH rather than 5-OH [13]. Thus, based on the ionic intensity and abundance, compounds **27**, **30**, and **44** were deduced to be 3-OH, 5-OH, and 4-OH esterified caffeoylquinic acids, respectively. Additionally, chlorogenic acids **22**, **26**, **32**, **45**, **54**, **80**, and **92** were identified using diagnostic ions and comparison with that of previous reports [12-13].

In the case of gallic acids exhibiting glycosyl substitution, the sugar units were initially cleaved in the MS/MS spectra, resulting in the base peak of gallic acid at *m/z* 169.01. However, the precise determination of glycosylation sites remained challenging based solely on the MS/MS spectrum. Therefore, compounds **6**, **11**, **16**, and **17** were provisionally characterized as diglucosyl gallic acid, 1'-*O*-galloylsucrose, 6'-*O*-galloylsucrose, and 6-*O*-galloylsucrose [15], respectively; compounds **10** and **13** were identified as gallic acid and its isomer, respectively.

Furthermore, based on the exact molecular weights, common fragmentation patterns, such as neutral losses of H_2O, CO, and CO_2, and comparison with that of the references [11-13], another seven phenolic acids (**20**, **21**, **23**, **24**, **28**, **31**, and **35**) were tentatively characterized in the CKF extracts.

Identification of chromones in CKF

Chromones are the major active ingredients in SR. In this study, eight chromones were identified from the CKF extracts, including four dihydrofuranchromones and four dihydropyranchromones. The MS/MS spectra exhibited distinctive fragmentation patterns, including common neutral losses of glucose, H_2O, CH_3, and CO. Additionally, RDA cleavages were observed in the dihydrofuran and dihydropyran rings [14].

Compound **88** exhibited a $[M + H]^+$ ion at *m/z* 453.1760, implying its molecular formula as $C_{22}H_{28}O_{10}$. The characteristic ions at *m/z* 291.1236 $[M + H - Glc]^+$, 273.1126 $[M + H - Glc - H_2O]^+$, and 219.0651 $[M + H - Glc - C_4H_8O]^+$ were observed, corresponding to the neutral losses of glucose, H_2O, and RDA cleavage [14]. Therefore, com-

pound **88** was identified as 5-*O*-methylvisammioside, which was further validated by comparison with that of the reference standard. Similarly, compounds **58** and **74** were accurately assigned as prim-*O*-glucosyl-cimifugin and cimifugin, respectively. Compound **118** displayed the same fragmentation behavior as that of **88**, except for the neutral loss of glucose. Consequently, it was tentatively characterized as 5-*O*-methylvisamminol.

Compound **127** exhibited a $[M + H]^+$ ion at *m/z* 439.1603, suggesting that its molecular formula is $C_{21}H_{26}O_{10}$. The MS/MS spectrum of compound **127** exhibited distinctive ions at *m/z* 277.1086 $[M + H - Glc]^+$, 259.0971 $[M + H - Glc - H_2O]^+$, and 205.0499 $[M + H - Glc - C_4H_8O]^+$, which align with the fragmentation pattern commonly observed for dihydrofuranchromones. Meanwhile, the presence of a fragment ion at *m/z* 217.0505 $[M + H - Glc - H_2O - C_3H_6]^+$ suggested the occurrence of neutral loss of C_3H_6, which could be attributed to the RDA cleavage of the dihydropyran ring leading to the formation of the corresponding furan ring [15]. Then, through comparison with a reference standard, compound **127** was unambiguously identified as sec-*O*-glucosylhamaudol. Based on molecular weights, neutral losses, and comparison with the related references [14, 15], other dihydropyranchromones (**136**, **147**, and **150)** were tentatively identified.

Identification of coumarins in CKF

Coumarins are one of the main ingredients in SR. The present investigation yielded the identification and characterization of 5 coumarins, classified as simple coumarins, furanocoumarins, and pyranocoumarins based on their distinctive parent structures. Through meticulous analysis involving the precise determination of molecular weights and observation of neutral losses resulting from side-chain substituents, compounds **39**, **130**, **135**, **146**, and **149** were tentatively characterized (Table S1 and Fig. S1).

Identification of iridoid glycosides and phenylethanoid glycosides in CKF

Iridoid glycosides and phenylethanoid glycosides are the main ingredients of RRP. In the current investigation, a comprehensive analysis of the CKF extracts revealed the presence of seven iridoid glycosides and seven phenylethanoid glycosides.

Iridoid glycosides exhibited a characteristic fragmentation pattern in the MS/MS spectrum, primarily involving the preferential cleavage of the glycosyl moiety, resulting in the generation of aglycone fragment ions. Additionally, frequent neutral losses of H_2O, CH_2O, and CO_2 were observed, indicating the presence of -OH, -CH_2OH, and -COOH, respectively, in their core structures. For example, compound **9** showed a pseudomolecular ion at *m/z* 407.1147 $[M + HCOO]^-$ and 361.1155 $[M - H]^-$, indicating its molecular formula as $C_{15}H_{22}O_{10}$. The corresponding MS/MS spectrum exhibited characteristic ions at *m/z* 343.1033 $[M - H - H_2O]^-$, 199.0610 $[M - H - C_6H_{10}O_5]^-$, and 169.0488 $[M - H - C_6H_{10}O_5 - CH_2O]^-$, indicative of the presence of -OH, -CH_2OH, and glycosyl units, respectively, in its structure. A comparison with a reference standard confirmed its unambiguous identification as catalpol. Similarly, compound **25** was confidently identified as leonuride. Furthermore, the structures of iridoid glycosides **4**, **7**, **18**, **19**, and **34** were tentatively elucidated based on their fragmentation behavior and comparison with that of references [16, 17].

Phenylethanoid glycosides are known to arise from the condensation of phenylethanol with sugar moieties, wherein the sugar chain is usually esterified with cinnamic acid or glycosylation with other sugar moieties. Compound **55**, for example, exhibited a $[M- H]^-$ ion at *m/z* 785.2502 and characteristic ions at *m/z* 623.2176 $[M - H - caffeoyl]^-$ and 477.1583 $[M - H - caffeoyl-Rha]^-$, indicating the presence of caffeoyl and rhamnose moieties. It was then unambiguously identified as echinacoside by comparison with that of the authentic standard. Based on the precise molecular weights,neutrallosses,aswellascomparisonwithrelevantreferences [16, 17], compounds **62**, **76**, **81**, **86**, **119**, and **126** were tentatively identified as phenylethanoid glycosides (Table S1).

Identification of N-acetyldopamine oligomers in CKF

N-acetyldopamine oligomers are the characteristic components of CP, characterized by the assembly of two or three dopamine units, culminating in the formation of the benzodioxane core skeleton. In this study, we reported the identification and characterization of six *N*-acetyldopamine oligomers were characterized from CKF extracts for the first time. The differentiation of these compounds relied on specific diagnostic ions, namely *m/z* 192.06 and 150.05, indicative of the acetamido-substituted benzodioxane and amino-substituted benzodioxane, respectively. Additionally, the investigation of neutral losses, encompassing dihydroxyphenyl, acetamide, and *N*-ethylacetamide, facilitated the identification of substituents within the benzodioxane structure. For example, compounds **71** and **82**, sharing the same molecular formula $C_{20}H_{22}N_2O_6$, displayed characteristic ions at *m/z* 192.06 and 150.05 in the MS/MS spectra, indicating that they were *N*-acetyldopamine oligomers (Fig. 3). Meanwhile, the fragment ions at *m/z* 328.118 and 269.079 substantiated the sequential losses of NH_2COCH_3 (Fig. 3). Thus, compounds **71** and **82** were tentatively characterized as *N*-acetyldopamine dimers [18]. Similarly, compounds **105**, **109**, **113**, and **117**, all exhibiting the same molecular formula $C_{30}H_{31}N_3O_9$, were found to be isomers. A detailed analysis of their high-energy spectra revealed the presence of a fragment ion at *m/z* 387.15 $[M + H - C_{10}H_9NO_3]^+$, aligning with the elemental composition of *N*-acetyldopamine dimers. Furthermore, the characteristic ions at *m/z* 192.06 and 150.05 were also observed. By comparison with that of references [18, 19], they were tentatively characterized as *N*-acetyldopamine trimers.

Identification of monoterpenes in CKF

Monoterpenes are the principal bioactive components of PRA. In this study, 33 monoterpenes were characterized and identified from CKF extracts, with a notable prevalence of paeoniflorin and its analogs within this chemical repertoire. Structurally, paeoniflorin consisted of a pinane skeleton with

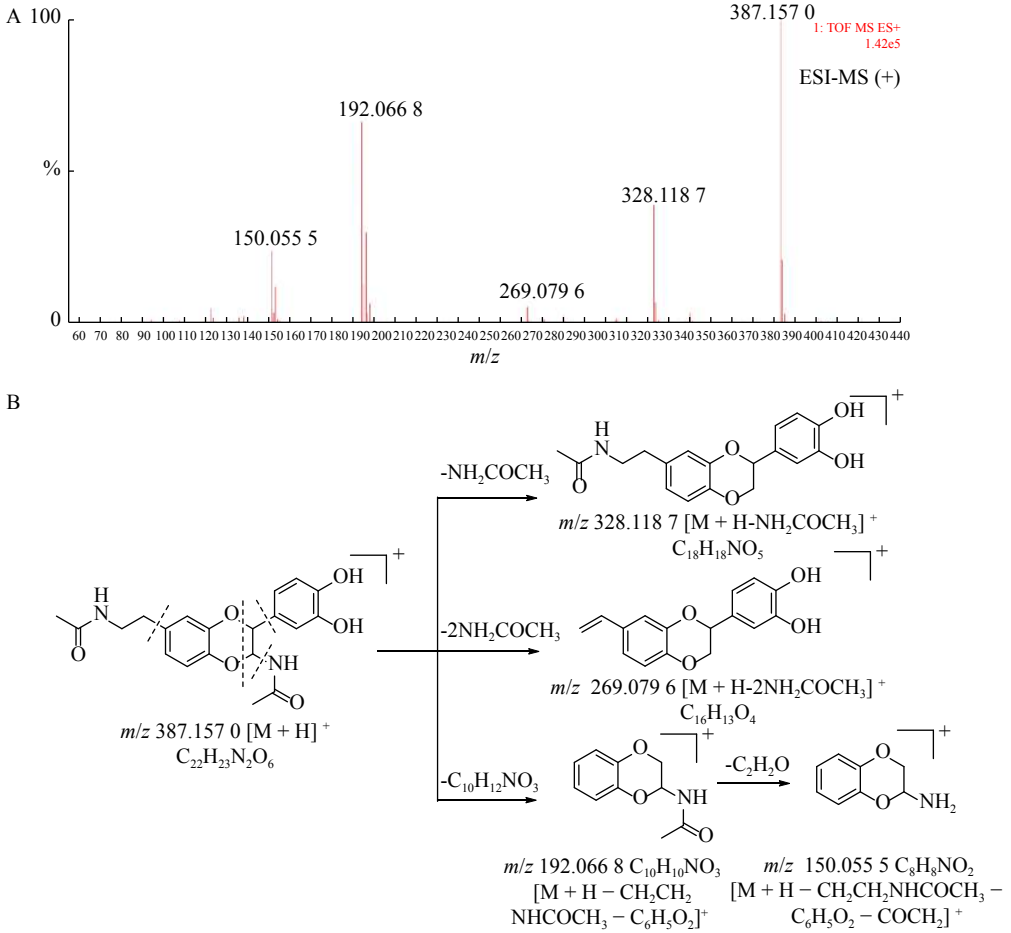

Fig. 3 The MS spectrum (A) and fragmentation pathways (B) of compound 71.

glucose, benzoic acid, and their derivatives. Due to the easy cleavage of ester and glycosidic bonds, we can identify the pinane skeleton at *m/z* 195.06 and 165.05 and characterize the substituents tethered to the pinane skeleton by scrutinizing the neutral losses. Remarkably, the recurring loss of CH_2O was frequently observed [20].

Compound **57** showed pseudomolecular ions at *m/z* 525.1619 $[M + HCOO]^-$ and 479.1570 $[M - H]^-$, indicating the molecular formula as $C_{23}H_{28}O_{11}$. The diagnostic ion at *m/z* 165.0556 $[C_9H_{10}O_3 - H]^-$ indicated the presence of a pinane skeleton. Moreover, the characteristic ions at *m/z* 449.1454 $[M - H - CH_2O]^-$, 345.1174 $[M - H - CH_2O - C_7H_4O]^-$, 327.1071 $[M - H - CH_2O - C_7H_6O_2]^-$, and 121.0294 $[M - H - C_6H_{10}O_5 - C_{10}H_{12}O_4]^-$ suggested the existence of benzoyl and glucosyl moieties. Thus, compound **57** was identified as paeoniflorin, which was confirmed by comparison with that of reference standards. Drawing upon the confluence of exact molecular weights, diagnostic ions, and discernible patterns of neutral loss, an array of structurally analogous compounds, namely compounds **8**, **36**, **37**, **46**, **48**, **50**, **56**, **59**, **70**, **73**, **89**, **93**, **101**, **104**, **110**, **and 112**, were tentatively characterized as derivatives of paeoniflorin. The assignment of their putative structures was consolidated through comprehensive comparisons with previously reported investigations [20, 21]. In addition, compounds **40** and **132** were unambiguously identified as oxypaeoniflorin and benzoylpaeoniflorin, respectively, by comparison with authentic standards.

Apart from paeoniflorin, albiflorin is another representative component in PRA. Albiflorin has a similar structure to that of paeoniflorin and also shows identical fragmentation behavior with that of paeoniflorin in the MS/MS spectrum. Here compound **52** was unambiguously identified to be albiflorin by comparing it with reference standards. Similarly, compounds **14**, **66**, **97**, **98**, **100**, **107**, and **133** were tentatively characterized as the analogs of albiflorin.

Furthermore, the structural elucidation of **33**, **42**, **53**, **91**, **124**, and **128** relied on a comprehensive analysis, incorporating their precise molecular weights, patterns of neutral loss, and comparison with relevant literature reports [20, 21].

Identification of resin glycosides in CKF

Resin glycosides, also known as glycolipids or lipo-oligosaccharides, constitute a distinctive group of compounds found in CS. These glycosides possess a rhamnose core structure, wherein two sugar chains are attached to positions C-1 and C-3, accompanied by two fatty acid chains at positions C-2 and C-4. In this investigation, a comprehensive analysis of CKF extracts led to the tentative identification of eight resin

glycosides. Notably, the fragmentation patterns observed in positive ion mode provided valuable insights for elucidating the sugar chains at positions C-1 and C-3, as well as determining the presence of short-chain fatty acids at position C-4. Meanwhile, in the negative ion mode, the base peak at *m/z* 271.22 or 243.19, generated from the loss of hydroxyl-substituted 16- or 14-carbon fatty acids, could be used to identify long-chain fatty acid at position C-2.

For example, compounds **138**−**140** had the same elemental composition of $C_{37}H_{66}O_{18}$ and produced diagnostic ions at *m/z* 243.19 in the MS/MS spectrum in the negative ion mode, indicating the presence of hydroxyl-substituted tetradecanoyl fatty acids at position C-2. In the positive ion mode, their fragmentation patterns revealed characteristic neutral losses of H_2O, glucosyl ($C_6H_{10}O_5$), rhamnosyl ($C_6H_{10}O_4$), and short-chain fatty acid ($C_5H_8O_2$), demonstrated the presence of glucosyl, rhamnosyl, and *α*-methyl-*β*-hydroxyl butyryl at positions C-1, C-3, and C-4, respectively. Thus, compounds **138**–**140** were tentatively identified as Cus-3/isomers. Compounds **141**–**143** and **145** (Fig. 4) exhibited $[M + H]^+$ ion at *m/z* 841.44 with the molecular formula of $C_{39}H_{68}O_{19}$, which was C_2H_2O more than that of Cus-3/isomers. Their MS/MS spectra displayed comparable fragmentation behaviors to compounds **138**–**140**, except for the neutral loss of acetylated glucosyl instead of glucosyl in the positive ion mode. This led to the generation of fragment ions at *m/z* 823.42 $[M + H - H_2O]^+$, 619.37 $[M + H - H_2O - C_8H_{12}O_6]^+$, 601.35 $[M + H - H_2O - C_8H_{12}O_6 - H_2O]^+$, 455.29 $[M + H - H_2O - C_8H_{12}O_6 - H_2O - C_6H_{10}O_4]^+$, and 355.24 $[M + H - H_2O - C_8H_{12}O_6 - H_2O - C_6H_{10}O_4 - C_5H_8O_2]^+$. Besides, the

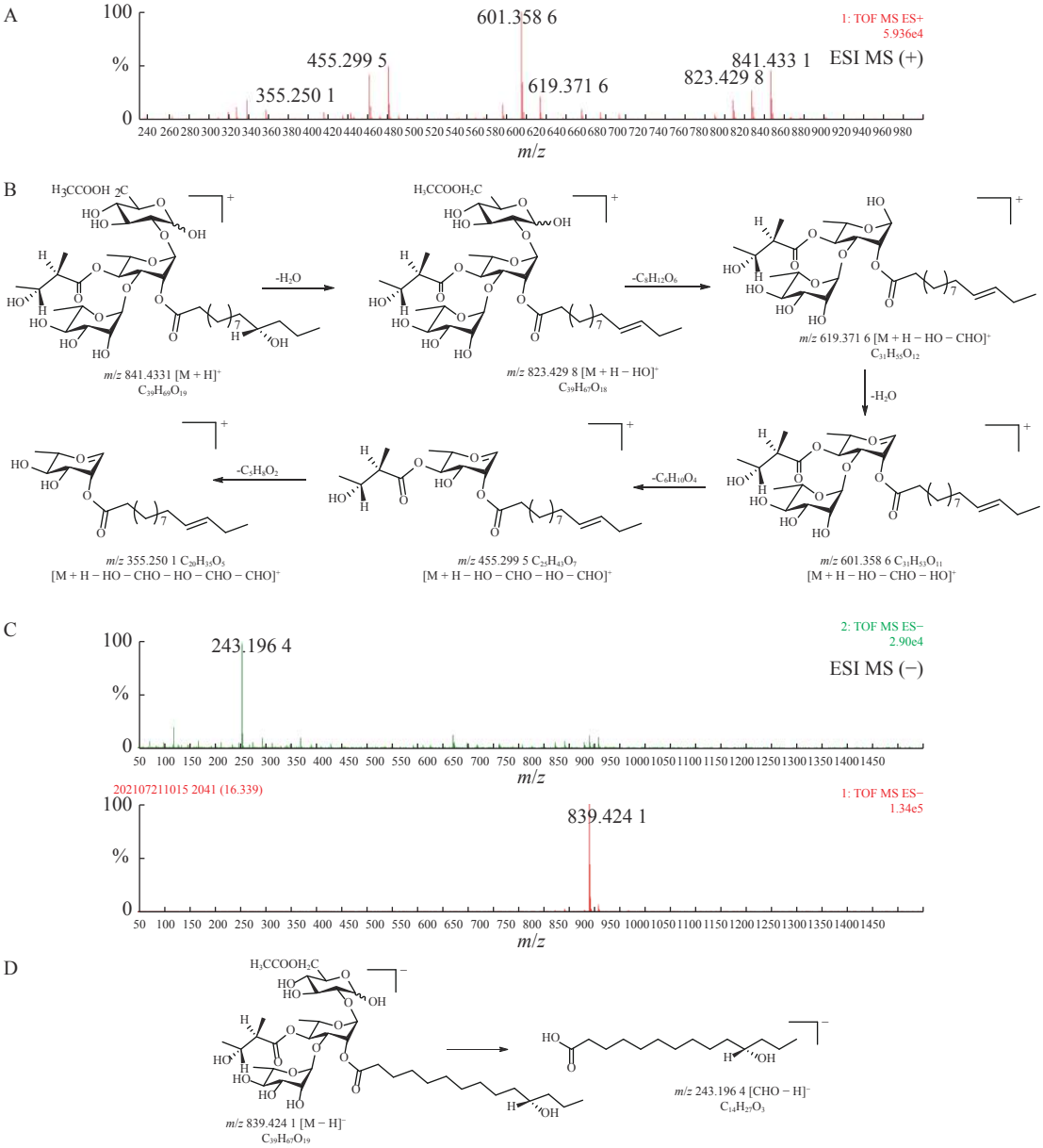

Fig. 4 The MS spectra and fragmentation pathways of compound 145 in the positive (A, B) and negative (C, D) ion modes.

diagnostic ion at *m/z* 243.19 was observed in the negative ion mode, indicating the presence of hydroxyl-substituted 14-carbon fatty acid. Thus, compounds **141**–**143** and **145** were tentatively characterized as Cus-1/isomers. In the high-energy spectrum of compound **148** ($C_{41}H_{72}O_{19}$), the diagnostic ion at *m/z* 271.2271 in the negative ion mode indicated the presence of hydroxyl-substituted 16-carbon fatty acid. Additionally, the same neutral losses as that of Cus-1/ isomer in the MS/MS spectrum in the positive ion mode were concluded by analyzing the fragment ions at *m/z* 851.4615 $[M + H - H_2O]^+$, 647.3964 $[M + H - H_2O - C_8H_{12}O_6]^+$, 629.3900 $[M + H - H_2O - C_8H_{12}O_6 - H_2O]^+$, 483.3315 $[M + H - H_2O - C_8H_{12}O_6 - H_2O - C_6H_{10}O_4]^+$, and 383.2787 $[M + H - H_2O - C_8H_{12}O_6 - H_2O - C_6H_{10}O_4 - C_5H_8O_2]^+$. Thus, compound **148** was speculatively characterized as Cus-2.

Identification of other types of components in CKF

In the present study, a total of nine additional compounds (**1**–**3**, **5**, **12**, **15**, **29**, **134**, and **137**) were tentatively characterized in the CKF extracts. Among them, three were from PRA, three were from RRP, two were from CS, and the remaining one was from FDR (Table S1).

Characterization of components in bio-samples of rats

Based on the data processing strategy, we first identified or tentatively characterized 190 xenobiotics from the bio-samples of SD rats treated with high-dose CKF extracts (Table S2 and S3). Then, the metabolic profile of CKF extracts administered at a normal dosage of 0.60 $g \cdot kg^{-1} \cdot d^{-1}$ was thoroughly examined, which resulted in the identification or tentative characterization of 149 xenobiotics, including 58 prototypes and 91 metabolites. Additionally, the contents of xenobiotics were positively correlated with the dosage administered to rats to a certain extent. All xenobiotics observed in the CKF normal-dose group were prominent constituents exhibiting relatively higher abundance compared to those identified in the CKF high-dose group.

Characterization of prototype components in CKF-treated bio-samples

According to the accurate molecular weights, retention time, and mass fragmentation behaviors of components in CKF extracts, we identified or tentatively characterized 58 prototypes in rat bio-samples, including 10 in plasma, 22 in urine, 21 in feces, 50 in intestinal contents, and 2 in the brain tissues. The detailed MS fragmentation information is displayed in Table S5.

Characterization of metabolites in CKF-treated bio-samples

Based on a comparative analysis of the total ion chromatogram (TIC) of rat bio-samples, blank samples, and CKF extracts, we identified a set of peaks exclusively present in the rat bio-samples, which were indicative of potential metabolites. A total of 91 metabolites were successfully identified or tentatively characterized within the CKF-treated bio-samples. These metabolites exhibited diverse distribution patterns across various biological matrices, comprising 20 in plasma, 47 in urine, 39 in feces, 49 in intestinal contents, and 2 in brain tissues, which can be classified into monoterpenes glycosides, phenolic acids, alkaloids, chromones, resin glycosides, and others, according to their structure types. The detailed MS fragmentation information is compiled in Table 1.

Characterization of monoterpenes-related metabolites

Nine monoterpenes-related metabolites were tentatively characterized from the bio-samples of SD rats treated with CKF extracts, which may be from paeoniflorin, benzoylpaeoniflorin, and albiflorin, the main monoterpenes in CKF formula. The metabolic pathways included methylation, hydroxylation, oxidation, sulfation, dehydration, and glucuronidation (Fig. 5).

Compound **M34** showed a $[M - H]^-$ ion at *m/z* 375.1300, corresponding to the molecular formula $C_{16}H_{24}O_{10}$, which was C_7H_4O (benzoyl unit) less than that of paeoniflorin. Besides, the characteristic ion at *m/z* 179.0563 $[C_6H_{12}O_6 - H]^-$ suggested the presence of a glucose moiety, while the neutral loss of 195.06 indicated the existence of a plane skeleton. Therefore, **M34** was tentatively identified as desbenzoylpaeoniflorin [22]. Notably, this metabolite was exclusively detected in the brain tissue among the monoterpenes-related metabolites. Compound **M6** showed a pseudomolecular ion at *m/z* 671.1876 $[M - H]^-$, indicating the molecular formula $C_{29}H_{36}O_{18}$, which was 192 Da more than that of paeoniflorin. The observed neutral loss of 176 Da, as inferred from the fragment ion at *m/z* 495.1483, indicated the presence of a glucuronide moiety. Besides, the characteristic ions at *m/z* 137.0251 suggested the presence of a *p*-hydroxybenzoyl group. Therefore, **M6** was speculated as a hydroxylated paeoniflorin glucuronide, with glucuronide and hydroxyl groups replacing the glucosyl and benzoyl groups, respectively, of the original structure. Compound **M13** exhibited a $[M - H]^-$ ion at *m/z* 527.1418, corresponding to the molecular formula $C_{23}H_{28}O_{14}$, which was 48 Da (3O) more than that of paeoniflorin. The characteristic ion at *m/z* 169.0147 $[C_7H_6O_5 - H]^-$ indicated the presence of a 3,4,5-trihydroxy benzoyl group. Thus, **M13** was tentatively characterized as a trihydroxylated derivative of paeoniflorin, with hydroxylation occurring in the benzoyl moiety of the structure. Similarly, six additional monoterpenes-related metabolites, including two methylated products (**M5** and **M82**), two sulfated products (**M36** and **M70**), one glucuronidation product (**M38**), and one dehydration product (**M53**), were tentatively characterized by comparing their tandem mass behaviors with those reported in previous studies [22, 23].

Characterization of phenolic acid-related metabolites

A total of 22 phenolic acid-related metabolites, comprising 18 chlorogenic acid-related metabolites and four gallic acid-related metabolites, were identified in this study. The metabolic transformations involved several processes, including hydrolysis, methylation, oxidation, reduction, and sulfation (Fig. 6). For example, the prototype 5-*O*-caffeoylglucosyl quinic acid was hydrolyzed to produce the intermediates 5-*O*-caffeoyl quinic acid, quinic acid, and caffeic acid (**M24**). Methylation of 5-*O*-caffeoyl quinic acid yielded **M40**, and subsequent Michael addition with cytosine produced metabolite **M60**. **M17** (t_R = 4.06 min, *m/z* 258.9909 $[M - H]^-$) ex-

Table 1 Characterization of metabolites in bio-samples of SD rats treated with normal-dose of CKF extracts

No.	t_R/min	formula	selected ion	Measured mass	Calculated mass	Mass error/ppm	MS fragment	Identification	Source
M1	1.10	$C_9H_{10}O_3$	$[M-H]^-$	165.0559	165.0552	4.24	135.0450	*p*-hydroxyphenylpropionic acid /isomers	IC
M2	2.20	$C_8H_8O_3$	$[M-H]^-$	151.0407	151.0395	7.94	123.0440	$C_8H_8O_3$ (*N*-acetyldopamine dimer -C_6H_5O-$CH_2CH_2NHCOCH_3$)	F
M3	2.27	$C_8H_8O_4$	$[M-H]^-$	167.0346	167.0344	1.20	124.0528	vanillic acid	U,F
M4	2.30	$C_{15}H_{20}O_{10}$	$[M-H]^-$	359.0988	359.0978	1.39	197.0461	desaturated catalpol	IC
M5	2.44	$C_{17}H_{26}O_{10}$	$[M-H]^-$	389.1481	389.1448	8.48	195.0673	$C_{17}H_{26}O_{10}$ (albiflorin-C_7H_4O + CH_2)	P,IC
M6	2.48	$C_{29}H_{36}O_{18}$	$[M-H]^-$	671.1876	671.1823	7.90	495.1483,165.0558,137.0251	hydroxylated paeoniflorin glucuronide	IC
M7	2.61	$C_8H_8O_8S$	$[M-H]^-$	262.9861	262.9862	−0.38	183.0282,168.0062,124.0167	3-hydroxy-5-methoxy-4-(sulfooxy)benzoic acid	P,U,IC
M8	2.70	$C_8H_{10}O_6S$	$[M-H]^-$	233.0101	233.0120	−8.15	153.0552	$C_8H_{10}O_6S$ (gallic acid + 2*CH_3-CO_2 + SO_3)	P,U,IC
M9	2.83	$C_8H_8O_4$	$[M-H]^-$	167.0358	167.0344	8.38	124.0512	vanillic acid	U
M10	3.00	$C_{10}H_{12}O_3$	$[M-H]^-$	179.0719	179.0708	6.14	178.0616,135.0808	methyl 2-ethoxybenzoate	U
M11	3.16	$C_{11}H_{11}NO_5$	$[M-H]^-$	236.0542	236.0559	−7.20	162.0317	caffeic acid glycine	F,IC
M12	3.22	$C_{10}H_{13}NO_3$	$[M+H]^+$	196.0965	196.0974	−4.59	154.0859,137.0616,119.0508	*N*-acetyldopamine	U,F
M13	3.28	$C_{23}H_{28}O_{14}$	$[M-H]^-$	527.1418	527.1401	3.22	497.1307,195.0667,169.0147	tri-oxidation paeoniflorin	IC
M14	3.38	$C_{16}H_{23}O_{10}$	$[M-H]^-$	375.1310	375.1291	5.06	361.1135	methylated catalpol	IC
M15	3.82	$C_9H_{10}O_7S$	$[M-H]^-$	261.0079	261.0069	3.83	181.0499,135.0444	dihydrocaffeic acid sulfonate	U,IC
M16	3.90	$C_{10}H_{11}NO_6S$	$[M-H]^-$	272.0229	272.0229	0.00	192.0659	dehydrogenated *N*-acetyldopamine sulfonate	P,U,IC
M17	4.06	$C_9H_8O_7S$	$[M-H]^-$	258.9909	258.9912	−1.16	179.0330,135.0436	caffeic acid sulfonate	P,IC
M18	4.18	$C_9H_{10}O_4$	$[M-H]^-$	181.0508	181.0501	3.87	137.0602	dihydrocaffeic acid	F
M19	4.22	$C_9H_9NO_3$	$[M-H]^-$	178.0519	178.0504	8.42	134.0613	hippuric acid	P,U,F,IC
M20	4.23	$C_{19}H_{22}NO_4$	$[M]^+$	328.1556	328.1549	2.13	283.0981,251.0705	demethylated magnoflorine	F
M21	4.29	$C_{10}H_{10}O_7S$	$[M-H]^-$	273.0068	273.0069	−0.37	193.0508,178.0278,134.0371	methylated caffeic acid sulfonate	P,U,IC
M22	4.30	$C_9H_{10}O_8S$	$[M-H]^-$	277.0016	277.0018	−0.72	197.0450,182.0203	3,5-dimethoxy-4-(sulfooxy)benzoic acid	P,U
M23	4.34	$C_{20}H_{22}NO_5$	$[M]^+$	356.1499	356.1498	0.28	338.1393,322.1076	2 reducted hydroxylated berberine	U,F,IC
M24	4.39	$C_9H_8O_4$	$[M-H]^-$	179.0354	179.0344	5.59	135.0443	caffeic acid	F,IC
M25	4.57	$C_{22}H_{24}O_{12}$	$[M-H]^-$	479.1182	479.1190	−1.67	303.0874,137.0244	methylated catechin glucuronide	U,IC
M26	4.64	$C_{16}H_{16}O_8$	$[M+H]^+$	337.0930	337.0923	2.08	317.0644	hydroxylated divaricatacid	U,F,IC
M27	4.65	$C_{26}H_{32}NO_{11}$	$[M]^+$	534.1988	534.1975	2.43	358.1654, 340.1550	3 reducted hydroxylated berberine glucuronide	U
M28	4.71	$C_{25}H_{28}NO_{11}$	$[M]^+$	518.1677	518.1662	2.89	342.1368, 324.1235, 308.0920	hydroxylated reducted demethyleneberberine glucuronide	U,IC
M29	4.78	$C_{16}H_{18}O_7$	$[M+H]^+$	323.1136	323.1131	1.55	305.1055,259.0616,235.0600	hydroxylated cimifugin	F,IC

YANG Fengge, *et al.* / *Chin J Nat Med*, 2023, **21**(6): 459-480

Continued

No.	t_R/min	formula	selected ion	Measured mass	Calculated mass	Mass error/ppm	MS fragment	Identification	Source
M30	4.91	$C_{25}H_{24}NO_{10}$	$[M]^+$	498.1421	498.1400	4.22	322.1055,307.0847	demethylatd berberine glucuronide	U,IC
M31	5.00	$C_{25}H_{24}NO_{10}$	$[M]^+$	498.1403	498.1400	0.60	322.1055,307.0834	demethylatd berberine glucuronide	U
M32	5.08	$C_{30}H_{30}NO_{16}$	$[M]^+$	660.1561	660.1565	−0.61	484.1275,308.0936	didemethylberberbine glucuronide	U
M33	5.10	$C_{20}H_{24}NO_5$	$[M]^+$	358.1641	358.1654	−3.63	342.1702, 282.0898	hydroxylated magnoflorine	F,IC
M34	5.11	$C_{16}H_{24}O_{10}$	$[M-H]^-$	375.1300	375.1291	2.40	345.1160,179.0563	desbenzoypaeoniflorin	B,U,F,IC
M35	5.26	$C_{16}H_{18}O_7$	$[M+H]^+$	323.1126	323.1131	−1.55	275.0556,247.0628	hydroxylated cimifugin	P,U,F,IC
M36	5.30	$C_{23}H_{28}O_{14}S$	$[M-H]^-$	559.1133	559.1122	1.97	479.1544,137.0239	oxypaeoniflorin sulfonate	U,IC
M37	5.32	$C_{26}H_{30}NO_{11}$	$[M]^+$	532.1807	532.1819	−2.25	356.1515,338.1410	2 reducted hydroxylated berberine glucuronide	U
M38	5.45	$C_{29}H_{38}O_{16}$	$[M+HCOO]^-$	687.2154	687.2136	2.62	641.2078,479.1546,435.1624,195.0654,121.0301	albiflorin glucose conjugation	IC
M39	5.57	$C_{16}H_{16}O_7$	$[M+H]^+$	321.0983	321.0974	2.80	303.0876,273.0398,249.0401	$C_{16}H_{16}O_7$ (5-*O*-methylvisamminol + oxidation)	P,U,F
M40	5.59	$C_{17}H_{20}O_9$	$[M-H]^-$	367.1027	367.1029	−0.54	193.0497,191.0565	methylated chlorogenic acid	U,IC
M41	5.61	$C_7H_{10}O_5$	$[M-H]^-$	173.0461	173.0450	6.36	155.0358,111.0456	shikimic acid	IC
M42	5.68	$C_9H_8O_3$	$[M-H]^-$	163.0399	163.0395	2.45	119.0504	coumaric acid	P,U,F,IC
M43	5.79	$C_9H_9NO_4$	$[M-H]^-$	194.0462	194.0453	4.64	135.0319	3-hydroxyhippuric acid	P,U
M44	5.99	$C_{15}H_{16}O_5$	$[M-H]^-$	275.0930	275.0919	4.00	260.0696,245.0436	demethylated 5-*O*-methylvisamminol	U,F
M45	6.01	$C_9H_8O_2$	$[M-H]^-$	147.0447	147.0446	0.68	103.0551	cinnamic acid	P,F
M46	6.11	$C_{18}H_{14}NO_4$	$[M]^+$	308.0920	308.0923	−0.97	280.0974,266.0816	demethylenecoptisine	U,F,IC
M47	6.13	$C_{22}H_{26}O_{12}$	$[M+H]^+$	483.1502	483.1503	−0.21	307.1190,259.0609,235.0616	cimifugin glucuronide	P
M48	6.14	$C_{16}H_{18}O_7$	$[M+H]^+$	323.1119	323.1131	−3.71	305.1019,275.0565,247.0627,232.0358	hydroxylated cimifugin	P,U,F,IC
M49	6.17	$C_{25}H_{26}NO_{10}$	$[M]^+$	500.1548	500.1557	−1.80	324.1244,308.0909	demethylated jatrorrhizine glucuronide	P,U,IC
M50	6.26	$C_9H_{10}O_3$	$[M-H]^-$	165.0551	165.0552	−0.61	121.0658	*p*-hydroxyphenylpropionic acid/isomers	P,U
M51	6.27	$C_{26}H_{28}NO_{10}$	$[M]^+$	514.1706	514.1713	−1.36	338.1416,323.1154,294.1129	jatrorrhizine-3-*O*-glucuronide	IC
M52	6.33	$C_{26}H_{28}NO_{10}$	$[M]^+$	514.1713	514.1713	0.00	338.1415,323.1154,294.1122	jatrorrhizine-3-*O*-glucuronide	P,U
M53	6.69	$C_{16}H_{22}O_9$	$[M-H]^-$	357.1205	357.1186	5.32	181.0865,175.0255	$C_{16}H_{22}O_9$ (albiflorin-C_7H_4O-H_2O)	IC
M54	6.69	$C_{25}H_{24}NO_{10}$	$[M]^+$	498.1404	498.1400	0.80	322.1075,307.0853	demethylatd berberine glucuronide	U,IC
M55	6.96	$C_{24}H_{22}NO_{10}$	$[M]^+$	484.1223	484.1244	−4.34	308.0918	di-demethylated berberine glucuronide	IC
M56	7.21	$C_{20}H_{18}NO_7$	$[M]^+$	384.1094	384.1083	2.86	366.0998,336.1243	3 hydroxylated berberine	F
M57	7.31	$C_{12}H_8O_8S$	$[M-H]^-$	310.9861	310.9862	−0.32	231.0298	hydroxylated xanthotixin sulfonate	U
M58	7.50	$C_{21}H_{22}NO_5$	$[M]^+$	368.1487	368.1498	−2.99	336.1237,320.0931,292.0974	hydroxylated palamatine	F
M59	7.56	$C_{19}H_{18}NO_4$	$[M]^+$	324.1237	324.1236	0.31	308.0925,280.0975,266.0811	demethyleneberberine	U,F
M60	7.71	$C_{20}H_{27}NO_{11}S$	$[M-H]^-$	488.1262	488.1227	7.17	387.1632,219.0506	methylated chlorogenic acid cysteine	IC
M61	7.74	$C_{20}H_{18}NO_5$		352.1204	352.1185	5.40	336.1226,320.0940,292.0950	hydroxylated berberbine	F,IC

Continued

No.	t_R/min	formula	selected ion	Measured mass	Calculated mass	Mass error/ppm	MS fragment	Identification	Source
M62	7.75	$C_{15}H_{14}O_7$	$[M-H]^-$	305.0673	305.0661	3.93	261.0761,235.0243,189.0197	demethylated divaricatacid	U
M63	8.06	$C_7H_6O_3$	$[M-H]^-$	137.0240	137.0239	0.73	93.0347	$C_7H_6O_3$ (gallic acid-2O)	P
M64	8.23	$C_{22}H_{24}NO_5$	$[M]^+$	382.1680	382.1654	6.80	368.1504, 352.1547,336.1248	methylated hydroxylated palamatine	F
M65	8.29	$C_{21}H_{20}NO_5$	$[M]^+$	366.1331	366.1341	−2.73	350.1392,334.1083	hydroxylated methylated berberine	F
M66	8.33	$C_{20}H_{16}NO_5$	$[M]^+$	350.1084	350.1028	16.00	336.1248,320.0938	dehydrogenated hydroxylated berberine	F
M67	8.46	$C_{14}H_{18}O_4$	$[M+H]^+$	251.1297	251.1283	5.57	233.1174,191.0698	hydrogenated nodakenein (+ 4H)	U
M68	8.56	$C_{26}H_{28}NO_{11}$	$[M]^+$	530.1662	530.1662	0.00	354.1341, 338.1025, 310.1077	hydroxylated jatrorrhizine glucuronide	U
M69	8.61	$C_{21}H_{20}NO_5$	$[M]^+$	366.1342	366.1341	0.27	334.1096	hydroxylated methylated berberine	F
M70	8.63	$C_{30}H_{32}O_{14}S$	$[M-H]^-$	647.1467	647.1435	4.94	567.1862,479.1549,121.0294	benzoylpaeoniflorin sulfonate	IC
M71	8.79	$C_{19}H_{16}NO_4$	$[M]^+$	322.1078	322.1079	−0.31	320.0931,278.0812,250.0882	demethylatd berberine	F
M72	9.74	$C_{21}H_{20}NO_4$	$[M]^+$	350.1405	350.1392	3.71	334.1081, 306.1129, 290.0817	dehydrogenated palamatine	F
M73	9.76	$C_{12}H_8O_5$	$[M+H]^+$	233.0460	233.0450	4.29	218.0209	hydroxylated xanthotixin	U
M74	9.90	$C_{20}H_{16}NO_4$	$[M]^+$	334.1105	334.1079	7.78	318.0779,290.0801	dehydrogenated berberine	F
M75	10.18	$C_{21}H_{22}NO_4$	$[M]^+$	352.1550	352.1549	0.28	336.1250,292.0983	methylated jatrorrhizine	U,F
M76	10.27	$C_{20}H_{18}NO_4$	$[M]^+$	336.1240	336.1236	1.19	320.0928,318.0787,292.0977,290.0817	dehydrogenated jatrorrhizine	P,F,IC,B
M77	10.53	$C_{19}H_{18}NO_5$	$[M]^+$	340.1192	340.1185	2.06	324.0861,282.0770	hydroxylated demethyleneberberine	U,IC
M78	11.19	$C_{22}H_{24}NO_4$	$[M]^+$	366.1695	366.1705	−2.73	352.1578,336.1251,320.0932,292.0972	methylated palamatine	F
M79	11.23	$C_{20}H_{16}NO_7$	$[M]^+$	382.0901	382.0927	−6.80	364.0789, 346.0713, 318.0763	3 hydroxylated methylated coptisine	U,F
M80	11.34	$C_{21}H_{24}O_{11}$	$[M+H]^+$	453.1369	453.1397	−6.18	277.1082	hamaudol-3-*O*-glucuronide	U,IC
M81	11.35	$C_{21}H_{20}NO_6$	$[M]^+$	382.1290	382.1291	−0.26	336.1234,320.0910	dihydroxylated methylated berberine	F
M82	11.63	$C_{17}H_{26}O_9$	$[M-H]^-$	373.1498	373.1499	−0.27	193.0853	$C_{17}H_{26}O_9$ (albiflorin-$C_7H_4O_2$ + CH_2)	U
M83	12.08	$C_{16}H_{14}O_6$	$[M+H]^+$	303.0884	303.0869	4.95	288.0656,273.0418,245.0443,217.0509	$C_{16}H_{14}O_6$ (5-*O*-methylvisammioside-$C_6H_{10}O_6$ + oxidation)	U
M84	12.22	$C_{21}H_{22}NO_4$	$[M]^+$	352.1555	352.1549	1.70	336.1247,292.0984	methylated jatrorrhizine	IC
M85	12.31	$C_{20}H_{18}NO_4$	$[M]^+$	336.1248	336.1236	3.57	320.0926,292.0974,278.0824	dehydrogenated jatrorrhizine	IC
M86	12.67	$C_{16}H_{12}O_7$	$[M-H]^-$	315.0521	315.0505	5.08	301.0327,151.0039	methylated quercetin	U
M87	13.04	$C_{20}H_{16}NO_6$	$[M]^+$	366.0963	366.0978	−4.10	350.1027, 336.0872,292.0985	2 hydroxylated methylated coptisine	F
M88	15.73	$C_{38}H_{66}O_{19}$	$[M-H]^-$	825.4054	825.4120	−8.00	243.1979	demethylated Cus-1/Isomer	IC
M89	15.90	$C_{39}H_{70}O_{20}$	$[M-H]^-$	857.4391	857.4382	1.05	243.1978	hydrated Cus-1/Isomer	IC
M90	16.04	$C_{37}H_{66}O_{19}$	$[M-H]^-$	813.4107	813.4120	−1.60	243.1969	hydroxylated Cus-3/Isomer	F,IC
M91	16.93	$C_{39}H_{68}O_{20}$	$[M-H]^-$	855.4233	855.4226	0.82	243.1958	hydroxylated Cus-1/Isomer	F,IC

P: Plasma; U: Urine; B: Brain; F: Feces; IC: Intestinal contents

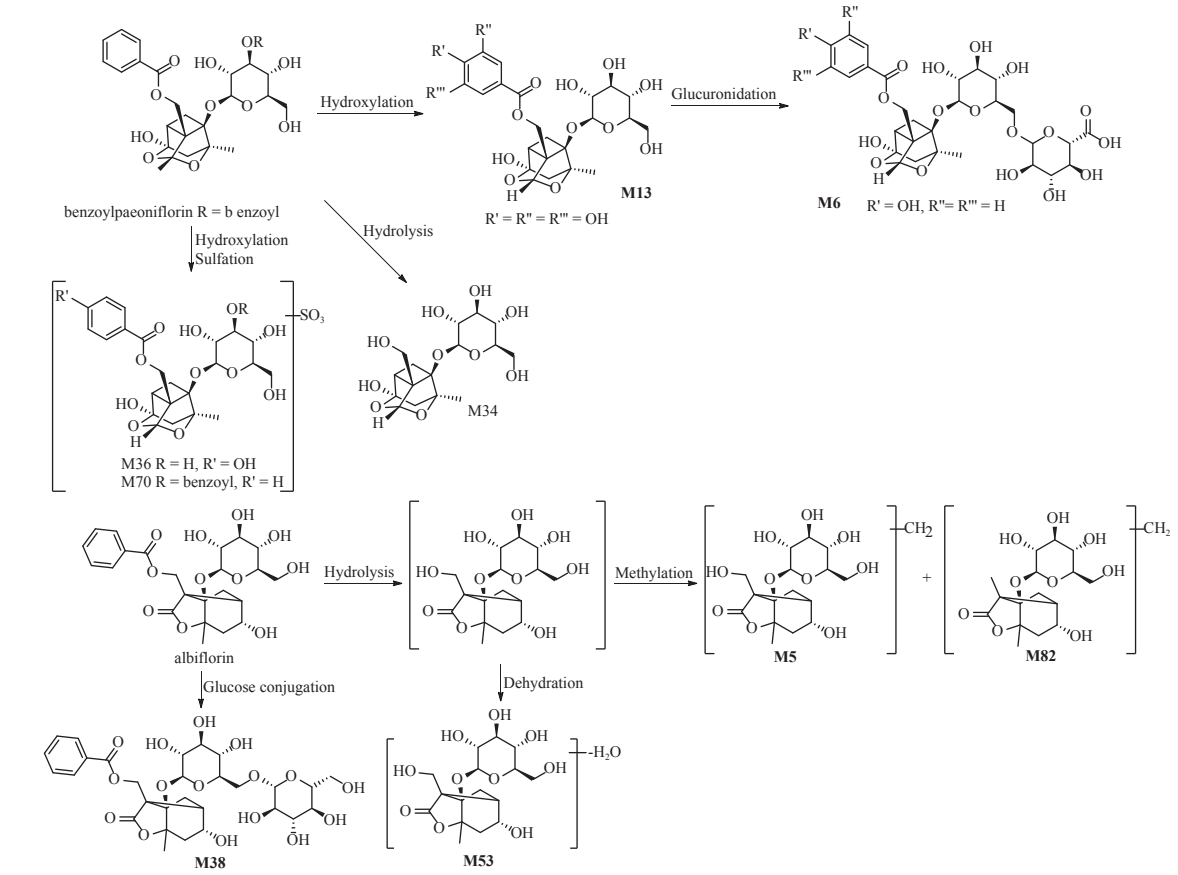

Fig. 5 The metabolic pathways of monoterpenes.

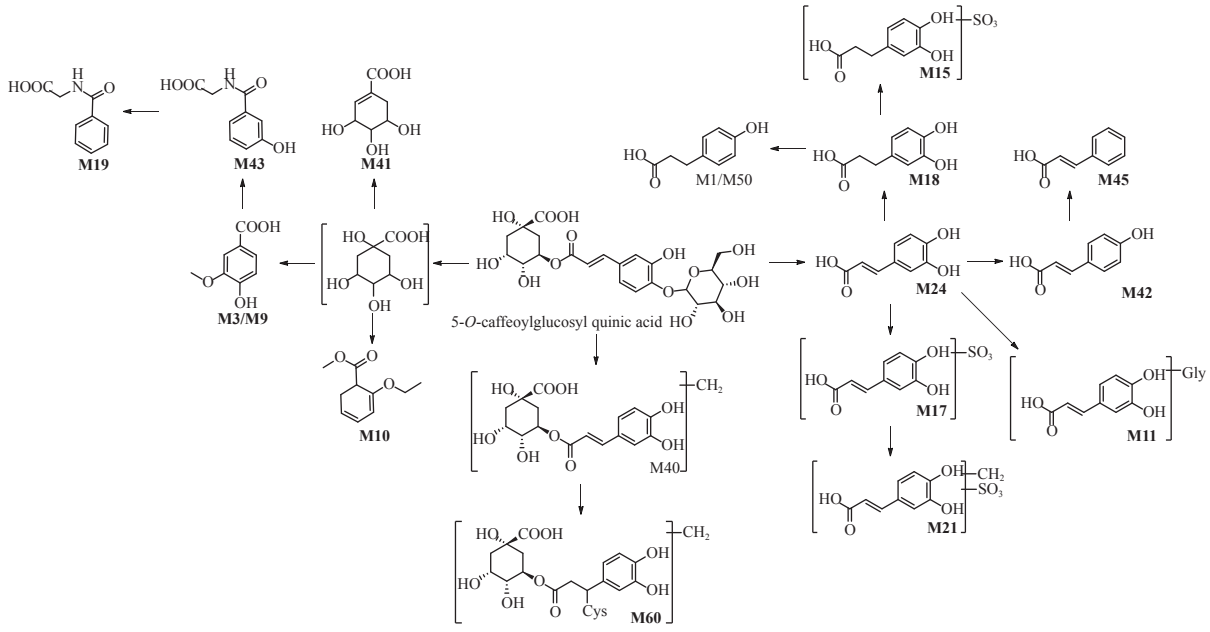

Fig. 6 The metabolic pathways of chlorogenic acids.

hibited the molecular formula $C_9H_8O_7S$, which was 80 Da higher than that of caffeic acid (**M24**). Fragment ions observed at *m/z* 179.0330 $[M - H - SO_3]^-$ and 135.0436 $[M - H - SO_3 - CO_2]^-$ indicated the presence of sulfonic and carboxyl groups. Hence, **M17** was plausibly identified as sulfonate of caffeic acid [24]. **M21**, with a molecular weight 14 Da higher than that of **M17**, was identified as a methylated sulfonate derivative of caffeic acid. Additionally, metabolites

M1/**M50**, **M15**, **M18**, **M42**, and **M45** were identified as the derivatives of caffeic acids (**M24**), while **M11** was characterized as the addition product of caffeic acid with glycine. **M10** and **M41** were identified as the derivatives of quinic acid. Dehydration and aromatization of quinic acid led to the formation of metabolites **M3**/**M9**. Furthermore, **M19** and **M43** were characterized as condensation products of benzoic acid with glycine.

Moreover, **M63** exhibited a quasi-molecular ion $[M-H]^-$ at *m/z* 137.0240 ($C_7H_6O_3$), which was 32 Da (2O) less than that of gallic acid, and yielded fragment ion at *m/z* 93.0347 $[M-H-CO_2]^-$. Therefore, it was identified as the dehydroxylated product of gallic acid. The other three gallic acid-related metabolites, **M7**, **M8**, and **M22**, were tentatively characterized through a comprehensive analysis of their accurate mass weights and fragmentation ions and comparison with those in previous reports [25, 26].

Characterization of chromone-related metabolites

In total, ten chromone-related metabolites were detected from the bio-samples of SD rats treated with CKF extracts. The metabolic transformations predominantly involved oxidation, hydroxylation, demethylation, and glucuronidation (Fig. 7).

M29, **M35**, and **M48** were deduced as hydroxylated cimifugin owing to their identical molecular formula of $C_{16}H_{18}O_7$, which differed by one additional oxygen atom compared with cimifugin. **M39** exhibited a $[M+H]^+$ ion at *m/z* 321.0983 ($C_{16}H_{16}O_7$), which was 30 Da (+ 2O − 2H) higher than that of 5-*O*-methylvisamminol, indicating the oxidation of the methyl group to the carboxyl group. The fragment ion at *m/z* 249.0401 $[M+H-C_4H_8O]^+$, corresponding to the RDA cleavage of the pyran ring, was 30 Da higher than that of 5-*O*-methylvisamminol, suggesting the occurrence of oxidation at the methyl group at position C-2. **M62** was the demethylation product of **M39** since its molecular formula, $C_{15}H_{14}O_7$, was CH_2 less than that of **M39**. Furthermore, **M62** exhibited a fragment ion at *m/z* 235.0243 $[M+H-C_4H_8O]^+$, 14 Da less than that of **M39**, which indicated that demethylation occurred at position C-5. By thoroughly examining the accurate molecular weights and fragment ions, several other chromone-related metabolites (**M26**, **M44**, **M47**, **M80**, and **M83**) were tentatively characterized [27-28].

Characterization of alkaloid-related metabolites

A comprehensive analysis of the bio-samples obtained from SD rats treated with CKF extracts led to the identification and tentative characterization of 36 alkaloid-related metabolites. These metabolites consisted of four palmatine-related, eight jatrorrhizine-related, three coptisine-related, two magnoflorine-related, and 19 berberine-related alkaloids. The results revealed that dehydrogenation, hydroxylation, methylation, demethylation, demethylenation, and glucuronidation were the principal metabolic pathways involved in their transformations [29-30].

M76 (*m/z* 336.1240 $[M]^+$) and **M85** (*m/z* 336.1248 $[M]^+$) showed the identical molecular formula $C_{20}H_{18}NO_4$, which was 2H less than that of jatrorrhizine. Fragmentation analysis of **M76** revealed ions at *m/z* 292.0977 $[M-CH_3-H-CO]^+$ and 290.0817 $[M-CH_3-H-2H-CO]^+$, indicating the presence of a methylenedioxy group at C-2 and C-3 and vicinal dimethoxy groups at C-9 and C-10. This suggests the release of 2H from the methyl and hydroxyl groups at C-2 and C-3. **M85** produced fragment ions at *m/z* 320.0926 $[M-CH_3-H]^+$, 292.0974 $[M-CH_3-H-CO]^+$, and 278.0824 $[M-CH_3-H-CO-CH_2]^+$, following a fragmentation pattern similar to that of jatrorrhizine. Thus, it can be concluded that 2H was eliminated from C-5 and C-6. The glucuronidation of jatrorrhizine resulted in the formation of metabolites **M51** and **M52**, which underwent subsequent demethylation and hydroxylation to yield **M49** and **M68**, respectively. Palmatine underwent dehydrogenation and hydroxylation, leading to the production of **M72** and **M58**, respectively. The methylation of palmatine gave rise to **M78**, which was fur-

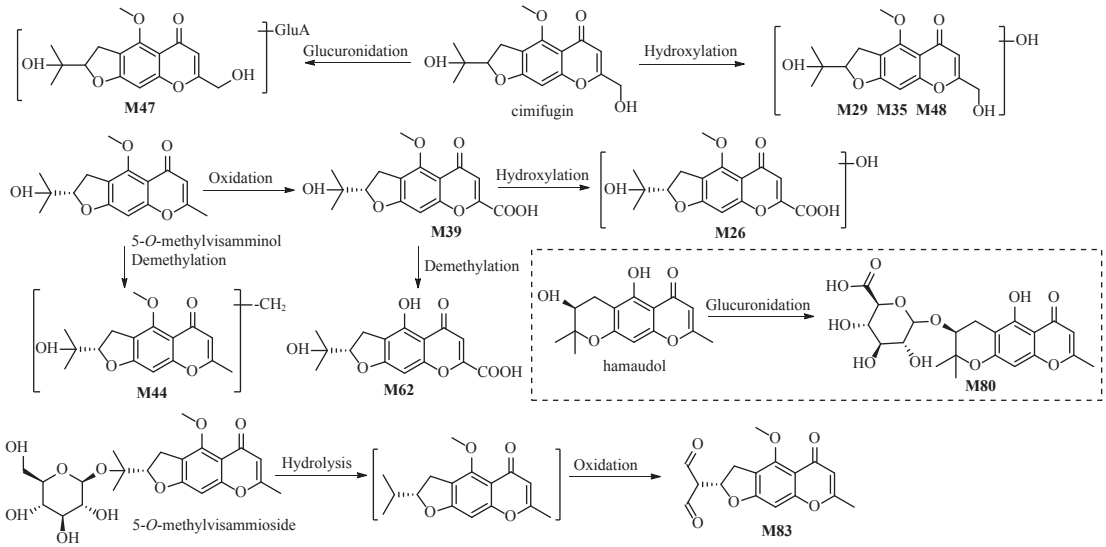

Fig. 7 The metabolic pathways of chromones.

ther hydroxylated to produce **M64**. **M46** was the demethylenated product of coptisine, while **M79** and **M87** were identified as the methylated and hydroxylated products of coptisine. **M20** and **M33** were the demethylated and hydroxylated products of magnoflorine, respectively.

Berberine underwent dehydrogenation to form **M74**, which was subsequently hydroxylated to produce **M66**. The demethylation of berberine resulted in the formation of **M71**, followed by glucuronidation and demethylation processes leading to the production of metabolites **M30**–**M32**, **M54**, and **M55**. The demethylenation of berberine yielded **M59**, which underwent hydroxylation to generate **M77**. The glucuronidation of **M77** gave rise to **M28**. The hydroxylation and hydrogenation of **M61** resulted in the formation of **M56** and **M23**, respectively. **M37** was the glucuronidation product of **M23**, and further hydrogenation led to the formation of **M27**. **M61** underwent monohydroxylation, followed by additional hydroxylation to yield the trihydroxylated product **M56**. The methylation of **M61** generated **M65** and **M69**, and subsequent methylation and hydroxylation led to the formation of **M81**.The proposed metabolic pathways are illustrated in Fig. 8.

Characterization of resin glycoside-related metabolites

In this study, we presented the novel characterization of resin glycosides derived from CKF extracts, a prominent constituent of CS. Additionally, we reported for the first time the identification and structural elucidation of four metabolites associated with resin glycosides in the bio-samples of SD rats treated with CKF extracts (Fig. 9). The observed metabolic transformations mainly involved demethylation, hydration, and hydroxylation.

M88 (t_R = 15.73 min) exhibited a pseudomolecular ion at *m/z* 825.4054 ($C_{38}H_{66}O_{19}$), which was 14 Da (CH_2) less than that of Cus-1/isomer. The MS/MS spectrum in the negative ion mode revealed a diagnostic ion at *m/z* 243.1979 $[C_{14}H_{28}O_3–H]^-$. Thus, **M88** was tentatively characterized as a demethylated derivative of Cus-1/isomer. Similarly, **M89** (t_R = 15.90 min, *m/z* 857.4391 $[M – H]^-$) was approximately assigned as the hydrated product of Cus-1/isomer. **M90** and **M91** displayed molecular formulas of $C_{37}H_{66}O_{19}$ and $C_{39}H_{68}O_{20}$, respectively, exhibiting a 16 Da increment relative to Cus-3/isomer and Cus-1/isomer. The diagnostic ion at

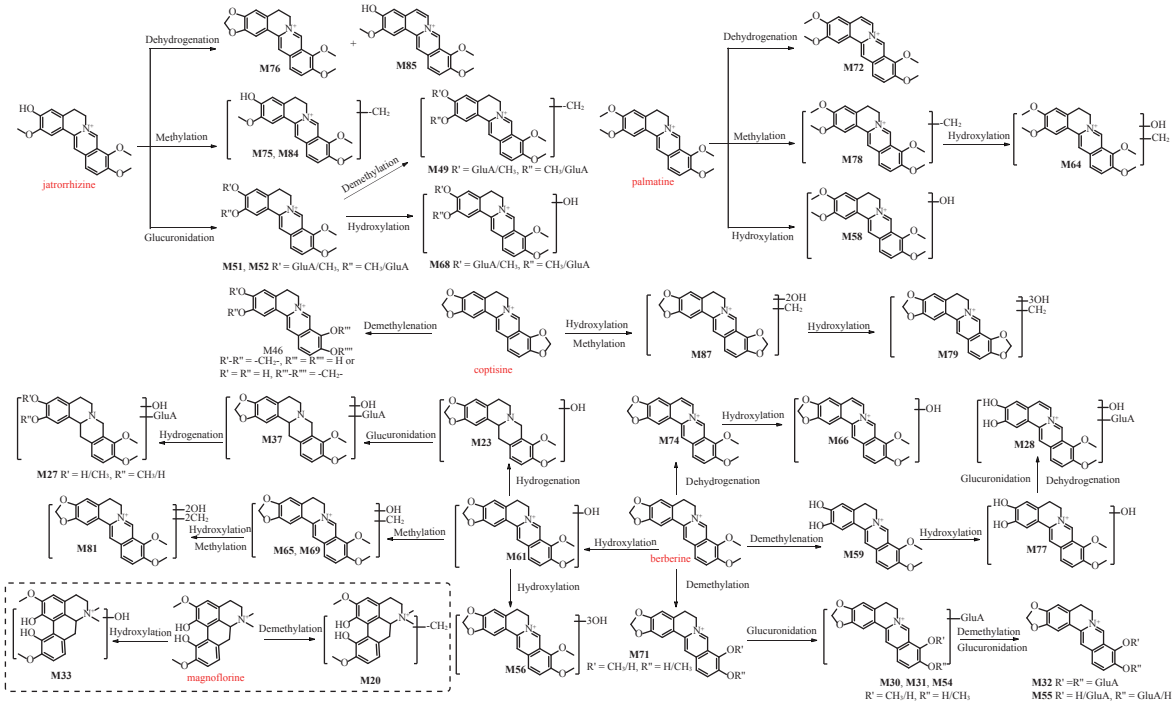

Fig. 8 The metabolic pathways of alkaloids.

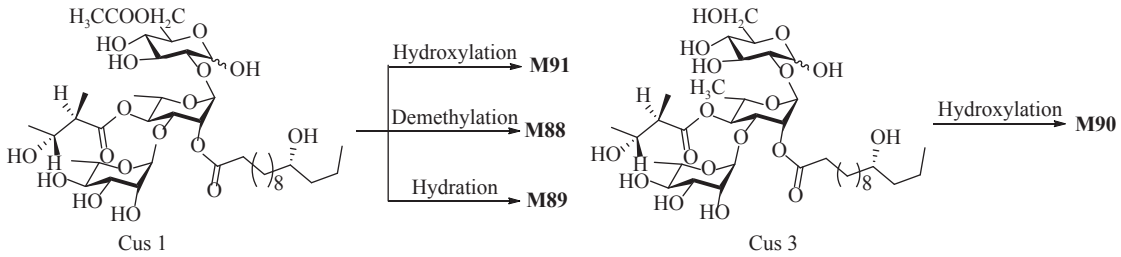

Fig. 9 The proposed metabolic pathways of resin glycosides.

m/z 243.19 was observed in the high-collision-energy scans of both metabolites. Hence, **M90** and **M91** were tentatively identified as hydroxylated products of Cus-3/isomer and Cus-1/isomer, respectively.

Characterization of N-acetyldopamine oligomer-related metabolites

In this study, we identified three *N*-acetyldopamine oligomer-related metabolites. **M12** showed a protonated ion at *m/z* 196.0965 ($C_{10}H_{13}NO_3$), in line with the molecular weight of *N*-acetyldopamine. Additionally, the fragment ions at *m/z* 154.0859 $[M+H-CH_2CO]^+$, 137.0616 $[M+H-NH_2COCH_3]^+$, and 119.0508 $[M + H- NH_2COCH_3- H_2O]^+$ further confirmed its identity as *N*-acetyldopamine, which is the first report of the metabolite detected from *N*-acetyldopamine oligomers. **M16** was proposed as a sulfated product of *N*-acetyldopamine analog. This proposition is based on the observation of the neutral loss of SO_3, as evidenced by the fragment ion at *m/z* 192.0659 $[M - H - SO_3]^-$. It is noteworthy that **M16** represents a novel metabolite derived from *N*-acetyldopamine oligomers. In addition, another *N*-acetyldopamine oligomer-related metabolite **M2** with a 1,4-dioxane core structure was also detected from the bio-samples, in line with previous reports [31]. The proposed metabolic pathways of *N*-acetyldopamine oligomers, involving RDA cleavage of the 1,4-dioxane and subsequent sulfation, are illustrated in Fig. 10.

Identification of potential targets of CKF for IBS treatment by network pharmacology

A total of 69 prototypes (**MOL1**–**MOL69**, Table S4) were identified in the bio-samples of SD rats treated with CKF extracts for investigating the potential targets and putative mechanism of the CKF formula in the treatment of IBS. The canonical SMILES chemical structures of the prototypes were obtained using ChemDraw 20.0, followed by target prediction through searches in the SEA and Swiss TargetPrediction databases. This analysis revealed 832 potential targets associated with the prototypes. Additionally, IBS-related targets were collected from the DisGeNET and GenCards databases, resulting in 561 targets related to the condition. By comparing the two target sets, we identified 130 targets that could potentially play a role in the treatment of IBS by the CKF formula (Fig. 11A). The PPI network of these targets was analyzed using the STRING database, and a comprehensive herb-component-target-disease network consisting of 203 nodes and 882 edges was constructed using Cytoscape (Fig. 11B). Subsequently, the vital parameters, including mean degree, BC, CC, EC, LAC, and NC, were calculated as 27, 0.00265, 0.4732, 0.05332, 6.3810, and 7.7667, respectively, according to established methods [32]. This process yielded 18 crucial targets for the CKF formula in the treatment of IBS (Fig. 11C). Furthermore, we conducted a KEGG pathways analysis of the 18 identified key targets, revealing the Top 20 signaling pathways involved (Fig. 11D). Among these pathways, ten were associated with diseases or substance dependence, such as Kaosi sarcoma-associated herpesvirus infection, Chagas disease, Human cytomegalovirus infection, Yersinia infection, Proteoglycans in cancer, pathways in cancer, pancreatic cancer, EGFR tyrosine kinase inhibitor resistance, Hepatitis B, and Coronavirus disease-COVID-19. One pathway was related to cellular processes (Focal adhesion), while five pathways were associated with signal transduction, including the PI3K-Akt signaling pathway, advanced glycation end-products (AGE)-receptor of AGE (RAGE) signaling pathway, HIF-1 signaling pathway, Rap1 signaling pathway, and vascular endothelial growth factor (VEGF) signaling pathway. Additionally, three pathways were classified as pattern recognition receptor (PRR) signaling pathways (C-type lectin receptor [CLR] signaling pathway, T cell receptor signaling pathway, and Toll-like receptor [TLR] signaling pathway), and one pathway was linked to inflammation (tumor necrosis factor [TNF] signaling pathway).

We found intriguing associations between the identified targets and pathways and inflammatory bowel disease (IBD), a gastrointestinal disorder characterized by recurrent inflammation of the intestinal tract due to an abnormal immune response to gut microflora. The pathogenesis and clinical manifestations of IBD share similarities with those of IBS. For example, accumulating evidence suggests the involvement of PRRs, such as CLRs and TLRs, in the pathogenesis of IBD [33]. Furthermore, the RAGE has been implicated in in-

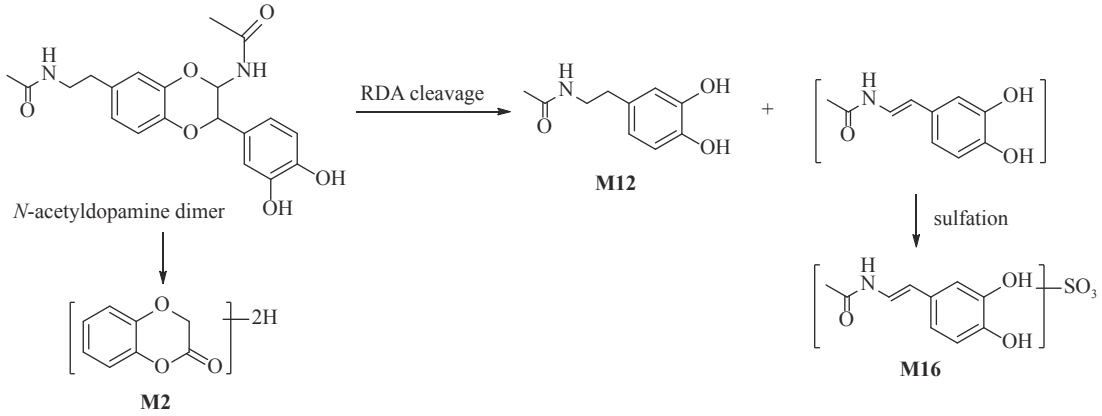

Fig. 10 The proposed metabolic pathways of *N*-acetyldopamine oligomers.

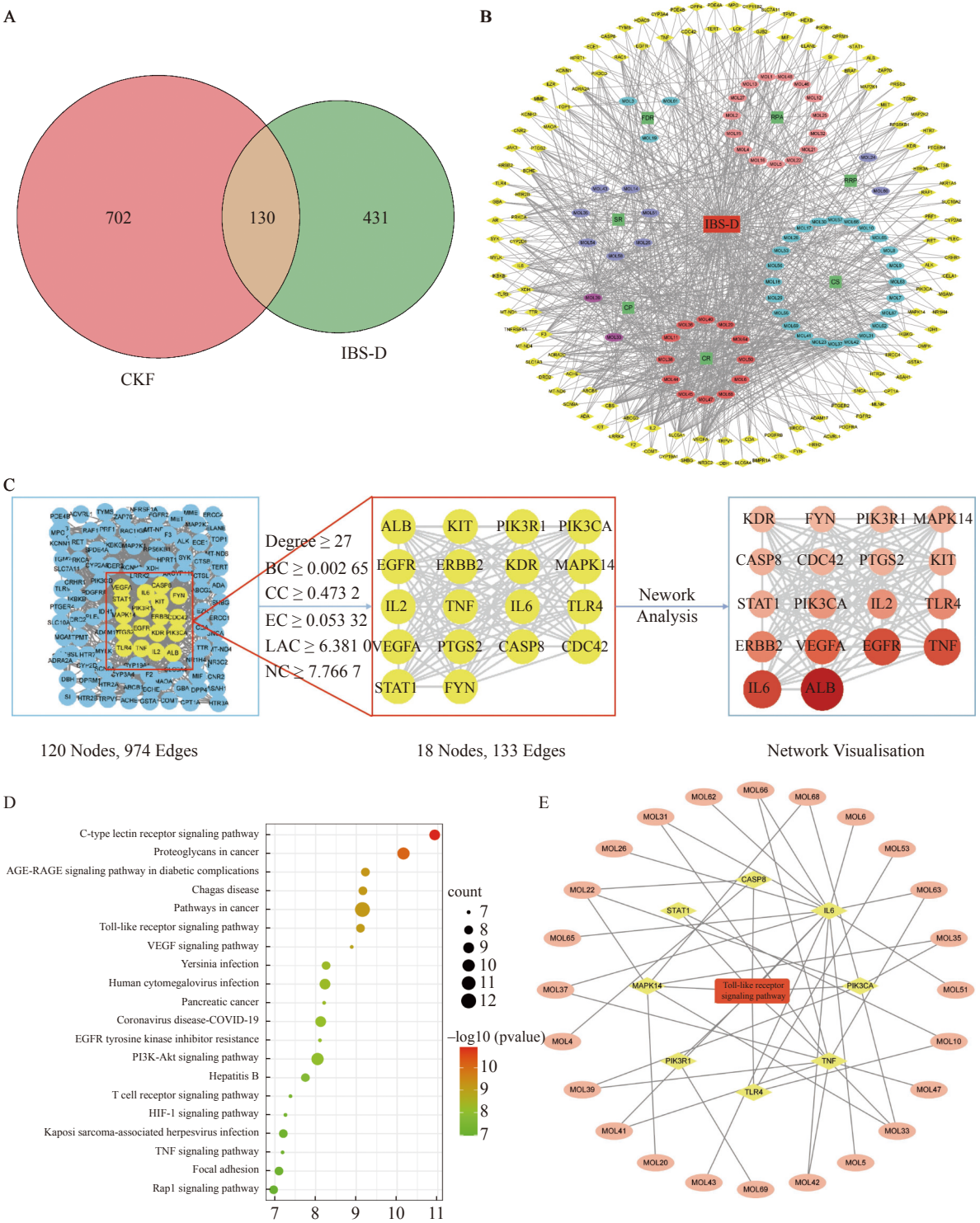

Fig. 11 CKF target prediction using network pharmacology. (A) Venn diagram of targets for the CKF formula in the treatment of IBS-D. (B) The network of "herb-component-target-disease". Red represents the disease IBS-D; green represents the herb names; yellow represents the targets; other colors represent the active components. PRA: Paeoniae Radix Alba, SR: Saposhnikoviae Radix, CR: Coptidis Rhizoma, CS: Cuscutae Semen, RRP: Rehmanniae Radix Praeparata, FDR: Fagopyri Dibotryis Rhizoma, CP: Cicadae Periostracum. (C) The PPI network analysis and recognition of core targets. The size of the nodes is proportional to their degrees in the map of Network Visualization. The node colors represent the average shortest path length. The larger the size, the longer the average shortest path length, and the darker the color, the higher the degree. (D) The KEGG enrichment pathway analysis of 18 core targets for the CKF formula in IBS-D treatment. The Y-axis represents significant pathways of the core targets, and the X-axis shows the *P* value. (E) Key component-target-pathway network for the Toll-like receptors signaling pathway.

flammatory responses and immune system activation in IBD, which can induce intestinal inflammation by promoting oxidative stress and endothelial activation and modulating gut permeability [34]. In addition, TNF, a downstream mediator of inflammation, is commonly targeted in the treatment of IBD. Recent reports have also highlighted the involvement of VEGF in IBD, as it regulates angiogenesis and may contribute to intestinal angiogenesis and mucosal inflammation [35].

Among the targets and signaling pathways associated with inflammatory intestinal diseases, TLRs stand out as a subject of considerable interest in IBS. TLRs have garnered attention due to their involvement in innate host defense mechanisms in the intestine, encompassing mucosal and commensal homeostasis [36]. Furthermore, these receptors play a pivotal role in modulating barrier function, visceral hypersensitivity, and other critical facets of IBS pathogenesis [37, 38]. Therefore, based on the TLRs signaling pathway, a key component-target-pathway network was constructed (Fig. 11E), suggesting that CASP8, IL6, MARK14, PIK3C, PIK3R1, STAT1, TLR4, and TNF may be significant therapeutic targets for the CKF formula and that the identified 24 components correlated with these targets may be active ingredients of the CKF formula in the treatment of IBS.

Molecular docking

To validate the findings obtained from network pharmacology, we conducted molecular docking simulations to investigate the binding interactions between 24 selected components and eight key targets in the TLRs signaling pathway. The docking scores, which indicate the binding affinity between the components and targets, revealed significant interactions between the selected targets, specifically TNF, MAPK14, TLR4, CASP8, PIK3CA, and PIK3R1, and the identified components, including alkaloids, flavonoids, chromones, monoterpenes, *N*-acetyldopamine dimers, *p*-hydroxycinnamic acid, and Cus-3/isomer (Fig. 12A). Further analysis of the binding modes revealed that **MOL39** (*N*-acetyldopamine dimer) formed hydrogen bonds with TYR-102, SER-118, and SER-120 of TLR4 (Fig. 12B); **MOL43** (5-*O*-methylvisammioside) formed a hydrogen bond with TYR-151 of TNF (Fig. 12C); **MOL51** (sec-*O*-glucosylhamaudol) formed hydrogen bonds with ASP-112 and ASP-168 to bind with MARK14 (Fig. 12D); **MOL65** (isorhamnetin-3-*O*-apiosyl-hexoside) formed hydrogen bonds with LEU-241, ILE-165, and PHE-170 to bind with CASP8 (Fig. 12E); **MOL68** (berberine) formed a hydrogen bond with TYR-836 to bind with PIK3CA and another hydrogen bond with ARG-951 to bind with PIK3R1 (Fig. 12F&12G). The results of molecular docking simulations are presented in Fig.12.

Discussion

The CKF formula, an established clinical intervention for IBS, holds promising potential; however, its material basis and underlying mechanism remain elusive, thereby restricting its widespread application. An essential aspect of TCM prescriptions lies in their chemical components, which serve as the fundamental contributors to their therapeutic efficacy. Thus, unraveling the comprehensive chemical profile of CKF becomes imperative. A previous study identified and characterized 80 chemical components derived from CKF extracts, encompassing six constituent herbal medicines, excluding CP [8]. In this study, 150 components were identified or tentatively characterized from CKF extracts, encompassing all seven constituent herbs. We also reported the characterization of six *N*-acetyldopamine oligomers from CP and eight resin glycosides from Corydalis yanhusuo in the CKF extracts, marking the first documentation of their presence in CKF. Noteworthy evidence suggests that *N*-acetyldopamine dimers possess potential therapeutic effects in attenuating LPS-induced inflammation and symptoms in male mouse models of ulcerative colitis induced by dextran sulfate sodium. These effects include mitigation of weight loss, tissue damage, and expression of proinflammatory cytokines[39,40]. In addition, resin glycosides exhibited antibacterial and antidepressant activities, as well as relaxant effects on rat ileum contractions [41,42]. These findings highlight the plausible association between resin glycosides and two crucial pathogenic factors of IBS, namely inflammation and brain-gut disorders.

According to the principles of plasma pharmacochemistry, potential bioactive components should be prototypes or related metabolites capable of being absorbed into the blood and maintaining a certain concentration in target organs. However, IBS is a complex intestinal disease involving dysregulation of the brain-gut axis, making it crucial to consider the presence of xenobiotics in brain tissue and intestinal contents. Meanwhile, the detection and chemical characterization of metabolites in urine and fecal samples were beneficial for understanding the *in vivo* metabolic pathways of CKF. Thus, bio-samples, including plasma, brain tissue, intestinal contents, and urine and fecal samples, were collected to investigate the metabolic behavior of CKF extracts. Our findings unveiled the presence of cimifugin and paeoniflorin in the plasma and brain tissues of rats subjected to CKF treatment. A previous report shows that chromones exhibit significant anti-inflammatory and analgesic activities [43], and their glucosides can ameliorate intestinal barrier dysfunction of Caco-2 cells by increasing the protein level of ZO-1 [44]. Meanwhile, it has been revealed that monoterpenes exhibit antidepressant and anti-inflammatory effects, and they can prevent intestinal barrier disruption [45-48]. Alkaloids, representative components of CR, were detected in the plasma of rats treated with CKF extracts. Studies have indicated that CR extracts can alleviate visceral pain in IBS model rats by reducing 5-HT and CCK levels [49] while also maintaining intestinal homeostasis by altering the abundance of related microbiota [50]. Flavonoids, abundant in intestinal contents, have been reported to possess anti-inflammatory properties, immune-regulating effects, and the ability to modulate gut microbiota [51, 52]. Additionally, *N*-acetyldopamine dimers and resin glycosides with high exposure in intestinal contents exhibited pronounced anti-inflammatory effects. Hence, it is plausible to consider these components as potential contributors to the synergistic effects observed in the treatment of IBS.

Network pharmacology, a powerful tool for interpreting

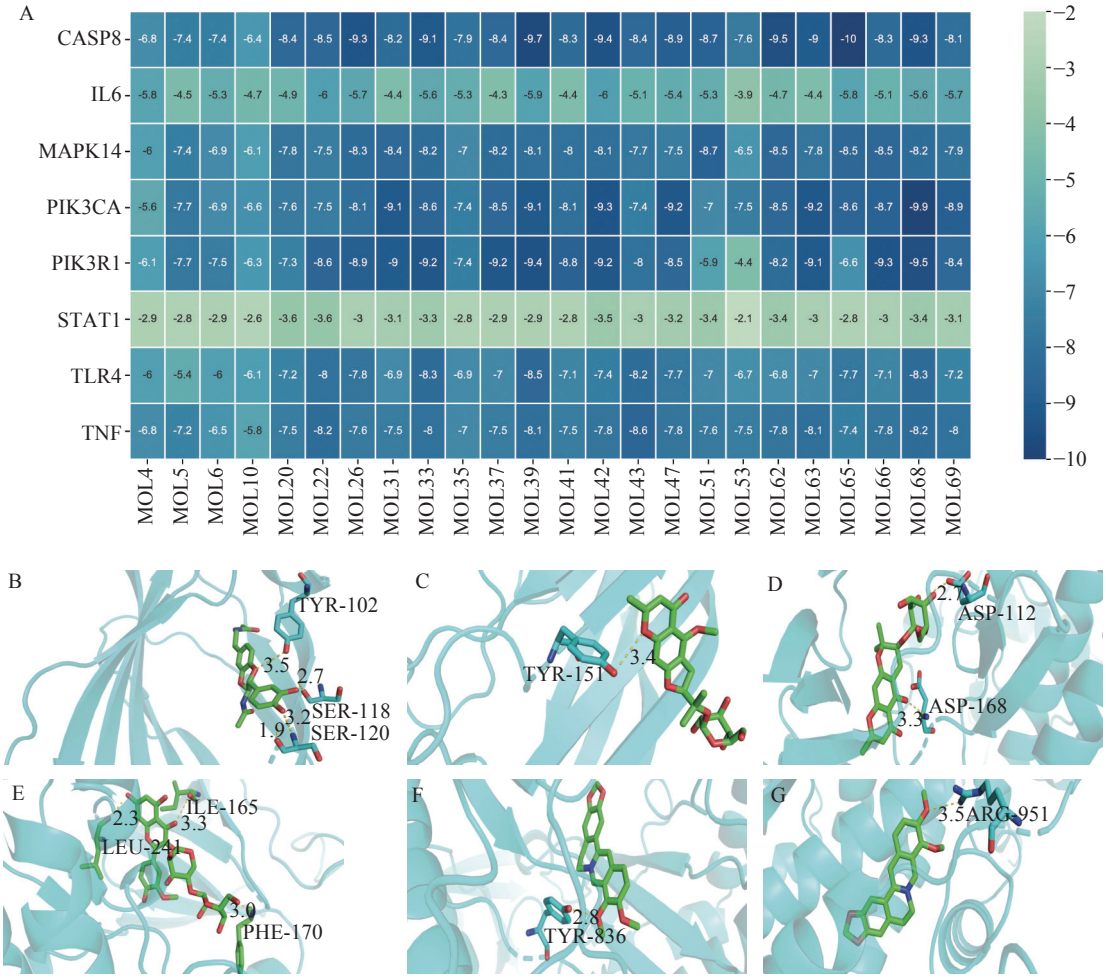

Fig. 12 Molecular docking results. (A) Binding energies between active components and targets. (B) A stable complex formed by MOL39 (*N*-acetyldopamine dimer) and TLR4. (C) A stable complex formed by MOL43 (5-*O*-methylvisammioside) and TNF. (D) A stable complex formed by MOL51 (sec-*O*-glucosylhamaudol) and MARK14. (E) A stable complex formed by MOL65 (isorhamnetin-3-*O*-apiosyl-hexoside) and CASP8. (F) A stable complex formed by MOL68 (berberine) and PIK3CA. (G) Stable complex formed by MOL68 (berberine) and PIK3R1.

complicated interactions from a systemic view, has been widely used to predict the main active ingredients and possible targets of TCM formulations [53]. In this study, our network pharmacology analysis identified 18 key targets and revealed 20 related pathways. As the TLR signaling pathway was associated with inflammation, immunity, epithelial cell proliferation and repair, barrier function, and visceral hypersensitivity, it was chosen for further molecular docking verification. Our results indicated that alkaloids, flavonoids, chromones, monoterpenes, *N*-acetyldopamine dimers, *p*-hydroxycinnamic acid, and Cus-3/isomer had high affinity with key targets related to the TLR signaling pathway, including MAPK14, TNF, TLR4, CASP8, PIK3CA, and PIK3R1. It has been reported that TLR4, MARK14, and TNF proteins are associated with inflammation [54,55], and CASP8, known as a protease regulating apoptosis and necroptosis, is involved in inflammation and gut homeostasis [56]. Additionally, PIK3C and PIK3R1 proteins, known to be correlated with colon cancer, may play an important role in IBS through immune and inflammation regulation [57,58]. These discoveries implied that the regulation of immune and inflammation may be the primary mechanism underlying the therapeutic effects of the CKF formula in the treatment of IBS.

Conclusion

In this study, a comprehensive analysis of CKF extracts led to the identification and tentative characterization of a total of 150 chemical components, with 23 components confirmed by comparison with reference standards. Notably, the discovery of six *N*-acetyldopamine oligomers from CP and eight resin glycosides from CS in the CKF extracts represents a novel finding. Additionally, we provided the MS/MS fragmentation patterns of resin glycosides for the first time. Moreover, 149 xenobiotics, including 58 prototypes and 91 metabolites, were qualitatively analyzed and characterized in the bio-samples of rats treated with the CKF extracts. This analysis enabled the initial profiling of the metabolic pathways associated with resin glycosides and *N*-acetyldopamine oligomers, leading to the detection and characterization of two new *N*-acetyldopamine dimer metabolites. In parallel, the

integrated application of network pharmacology and molecular docking technology was employed to explore the underlying mechanism of the CKF formula in the treatment of IBS. Our results revealed that alkaloids, flavonoids, chromones, monoterpenes, *N*-acetyldopamine dimers, *p*-hydroxycinnamic acid, and Cus-3/isomer may be the components responsible for the therapeutic effects of CKF. Furthermore, the TLR signaling pathway, implicated in inflammation and immunological processes, emerged as a potential modulatory target. To sum up, the chemical and metabolic profiles of CKF extracts were deciphered by UPLC-Q-TOF-MS/MS. In addition, the active components and underlying mechanisms of the CKF formula were elucidated through network pharmacology and subsequent molecular docking analyses. The findings of this study contribute to the understanding of the pharmacodynamic material basis of the CKF formula, laying the groundwork for further research on its mechanism of action and quality control in the treatment of IBS.

References

[1] Holtmann GJ, Ford AC, Talley NJ. Pathophysiology of irritable bowel syndrome [J]. *Lancet Gastroenterol Hepatol*, 2016, **1**(2): 133-146.

[2] Chey WD, Kurlander J, Eswaran S. Irritable bowel syndrome: a clinical review [J]. *JAMA*, 2015, **313**(9): 949-958.

[3] Defrees DN, Bailey J. Irritable bowel syndrome: epidemiology, pathophysiology, diagnosis, and treatment [J]. *Prim Care*, 2017, **44**(4): 655-671.

[4] Camilleri M, Lasch K, Zhou W. Irritable bowel syndrome: methods, mechanisms, and pathophysiology. The confluence of increased permeability, inflammation, and pain in irritable bowel syndrome [J]. *Am J Physiol Gastrointest Liver Physiol*, 2012, **303**(7): G775-785.

[5] Munjal A, Dedania B, Cash B. Update on pharmacotherapy for irritable bowel syndrome [J]. *Curr Gastroenterol Rep*, 2019, **21**(6): 25.

[6] Cao XL, Lu M. Clinic study on Changkang Fang treating irritable bowel syndrome [J]. *J Nanjing Univ Tradit Chin Med*, 2014, **30**(03): 232-234.

[7] Gao Q, Han ZY, Tian DF, *et al*. Xinglou Chengqi Decoction improves neurological function in experimental stroke mice as evidenced by gut microbiota analysis and network pharmacology [J]. *Chin J Nat Med*, 2021, **19**(2): 881-899.

[8] Mao Q, Shi L, Wang ZG, *et al*. Chemical profiles and pharmacological activities of Chang-Kang-Fang, a multi-herb Chinese medicinal formula, for treating irritable bowel syndrome [J]. *J Ethnopharmacol*, 2017, **201**: 123-135.

[9] Sneha Singh, Nandini Pathak, Eram Fatima, *et al*. Plant isoquinoline alkaloids: Advances in the chemistry and biology of berberine [J]. *Eur J Med Chem*, 2021, **226**: 11839.

[10] Li YY, Guo MQ, Li XM, *et al*. Simultaneous Qualitative and Quantitative Evaluation of the Coptidis Rhizoma and Euodiae Fructus Herbal Pair by Using UHPLC-ESI-QTOF-MS and UHPLC-DAD [J]. *Molecules*, 2020, **25**(20): 4782.

[11] Ye M, Yan Y, Guo DA. Characterization of phenolic compounds in the Chinese herbal drug Tu-Si-Zi by liquid chromatography coupled to electrospray ionization mass spectrometry [J]. *Rapid Commun Mass Spectrom*, 2005, **19**(11): 1469-1484.

[12] Gobbo-Neto L, Lopes NP. Online identification of chlorogenic acids, sesquiterpene lactones, and flavonoids in the Brazilian arnica Lychnophora ericoides Mart. (Asteraceae) leaves by HPLC-DAD-MS and HPLC-DAD-MS/MS and a validated HPLC-DAD method for their simultaneous analysis [J]. *J Agric Food Chem*, 2008, **56**(4): 1193-1204.

[13] Ncube EN, Mhlongo MI, Piater LA, *et al*. Analyses of chlorogenic acids and related cinnamic acid derivatives from *Nicotiana tabacum* tissues with the aid of UPLC-QTOF-MS/MS based on the in-source collision-induced dissociation method [J]. *Chem Cent J*, 2014, **8**(1): 66.

[14] Liu YJ, Ren XL, Huo JH, *et al*. Analysis on constituents of chromone in Fangfeng by UPLC-Q-TOF/MS [J]. *Chin J Tradit Med Sci Tech*, 2018, **25**(03): 355-361 + 384.

[15] Chen L, Chen X, Su L, *et al*. Rapid characterisation and identification of compounds in *Saposhnikoviae* Radix by high-performance liquid chromatography coupled with electrospray ionisation quadrupole time-of-flight mass spectrometry [J]. *Nat Prod Res*, 2018 , **32**(8): 898-901.

[16] Zhao XF, Li P, Sun LQ, *et al*. HPLC/ESI-MS analysis of the Radix *Rehmanniae Praeparata* [J]. *Chin J Pharm Anal*, 2007, (06): 874-876.

[17] Zhang YB, Jiang ZZ, Wang YF, *et al*. Analysis of chemical constituents in fresh, dried and prepared *Rehmanniae* Radix by UPLC/ESI-Q-TOF MS [J]. *Chin Tradit Pat Med*, 2016, **38**(05): 1104-1108.

[18] Cao XC, Zhang XY, Xu JD, *et al*. Quality consistency evaluation on four origins of *Cicadae Periostracum* by ultra-performance liquid chromatography coupled with quadrupole/time-of-flight mass spectrometry analysis [J]. *J Pharm Biomed Anal*, 2020, **179**: 112974.

[19] Matsumoto H, Konno K, Kazuma K. A comprehensive LC-MS and isolation study of cicada slough as a crude drug [J]. *Nat Prod Commun*, 2017, **12**(11): 1934578X1701201136.

[20] Yang S, Zhang X, Dong Y, *et al*. Cleavage rules of mass spectrometry fragments and rapid identification of chemical components of Radix *Paeoniae Alba* using UHPLC-Q-TOF-MS [J]. *Phytochem Anal*, 2021, **32**(5): 836-849.

[21] Li SL, Song JZ, Choi FF, *et al*. Chemical profiling of Radix *Paeoniae* evaluated by ultra-performance liquid chromatography/photo-diode-array/quadrupole time-of-flight mass spectrometry [J]. *J Pharm Biomed Anal*, 2009, **49**(2): 253-266.

[22] Cao W, Wang X, Li H, *et al*. Studies on metabolism of total glucosides of paeony from *Paeoniae* Radix Alba in rats by UPLC-Q-TOF-MS/MS [J]. *Biomed Chromatogr*, 2015, **29**(11): 1769-1779.

[23] Chen ZW, Tong L, Li SM, *et al*. Identification of metabolites of Radix *Paeoniae Alba* extract in rat bile, plasma and urine by ultra-performance liquid chromatography-quadrupole time-of-flight mass spectrometry [J]. *J Pharm Anal*, 2014, **4**(1): 14-25.

[24] Zhang FX, Xie ZN, Tang XY, *et al*. A combination of representative compounds, metabolism platform and diagnostic extraction strategy for characterization of metabolites of Shuang-Huang-Lian oral liquid *in vivo* by ultra-performance liquid chromatography coupled with time-of-flight mass spectrometry [J]. *J Pharm Biomed Anal*, 2018, **155**: 216-234.

[25] Azuma K, Ippoushi K, Nakayama M, *et al*. Absorption of chlorogenic acid and caffeic acid in rats after oral administration [J]. *J Agric Food Chem*, 2000, **48**(11): 5496-5500.

[26] Li WL, Zhang Y, Mu YY, *et al*. Identification of estrogenic constituents in serum after oral administration of Tu-Si-Zi extract using HPLC-ESI/Q-TOF MS/MS [J]. *J Liq Chromatogr Relat Technol*, 2015, **38**(16): 1521-1525.

[27] Li Y, Zhao L, Lv D, *et al*. Rapid analysis of *Saposhnikovia divaricate* decoction metabolism in rats by UHPLC-Q-TOF-MS and multivariate statistical analysis [J]. *Biomed Chromatogr*, 2020, **34**(3): 4778-4793.

[28] Li YY, Zhang B, Yuan YF. Identification of components and metabolites of *Saposhnikoviae* Radix decoction in rats plasma by UPLC-Q-TOF-MS [J]. *J Phar Pract*, 2019, **37**(6): 512-517.

[29] Feng X, Wang K, Hu X, *et al*. Systematic screening and characterization of absorbed constituents and *in vivo* metabolites in rats' after oral administration of Rhizoma *coptidis* using UPLC-Q-TOF/MS [J]. *Biomed Chromatogr*, 2020, **34**(10): e4919.

[30] Liu Y, Zhang Y, Meng Q, *et al*. Metabolic profile of alkaloids

in Rhizoma *Coptidis* in rat plasma, urine and feces after oral administration using ultra-high-performance liquid chromatography coupled with quadrupole time-of-flight mass spectrometry [J]. *Rapid Commun Mass Spectrom*, 2020, **34**(9): e8763.
[31] Cao XC, Guo MF, Han Y, *et al*. Systematic metabolite profiling of *N*-acetyldopamine oligomers from *Cicadae Periostracum* in rats by ultra-high performance liquid chromatography coupled with quadrupole-time-of-flight mass spectrometry [J]. *J Pharm Biomed Anal*, 2021, **192**: 113665.
[32] Chen Y, Chu F, Lin J, *et al*. The mechanisms of action of WeiChang'An Pill (WCAP) treat diarrhoea-predominant irritable bowel syndrome (IBS-D) using network pharmacology approach and *in vivo* studies [J]. *J Ethnopharmacol*, 2021, **275**: 114119.
[33] Walsh D, McCarthy J, O'Driscoll C, *et al*. Pattern recognition receptors-molecular orchestrators of inflammation in inflammatory bowel disease [J]. *Cytokine Growth Factor Rev*, 2013, **24**(2): 91-104.
[34] Body-Malapel M, Djouina M, Waxin C, *et al*. The RAGE signaling pathway is involved in intestinal inflammation and represents a promising therapeutic target for inflammatory bowel diseases [J]. *Mucosal Immunol*, 2019, **12**(2): 468-478.
[35] Scaldaferri F, Vetrano S, Sans M, *et al*. VEGF-A links angiogenesis and inflammation in inflammatory bowel disease pathogenesis [J]. *Gastroenterology*, 2009, **136**(2): 585-595.
[36] Cario E. Toll-like receptors in inflammatory bowel diseases: a decade later [J]. *Inflammatory Bowel Dis*, 2010, **16**(9): 1583-1597.
[37] Hyland NP, Quigley EMM, Brint E. Microbiota-host interactions in irritable bowel syndrome: epithelial barrier, immune regulation and brain-gut interactions [J]. *World J Gastroenterol*, 2014, **20**(27): 8859-8866.
[38] Lim KH, Staudt LM. Toll-like receptor signaling [J]. *Cold Spring Harbor Perspect Biol*, 2013, **5**(1): a011247-a011247.
[39] Xu MZ, Lee WS, Han JM, *et al*. Antioxidant and anti-inflammatory activities of *N*-acetyldopamine dimers from *Periostracum Cicadae* [J]. *Bioorg Med Chem*, 2006, **14**(23): 7826-7834.
[40] Huang LJ, Wang YM, Gong LQ, *et al*. *N*-Acetyldopamine dimer attenuates DSS-induced ulcerative colitis by suppressing NF-κB and MAPK pathways [J]. *Front Pharmacol*, 2022, **13**: 842730.
[41] León-Rivera I, Mirón-López G, Molina-Salinas GM, *et al*. Tyrianthinic acids from *Ipomoea tyrianthina* and their antimycobacterial activity, cytotoxicity, and effects on the central nervous system [J]. *J Nat Prod*, 2008, **71**(10): 1686-1691.
[42] Kitagawa I, Baek NI, Kawashima K, *et al*. Indonesian medicinal plants. XV. chemical structures of five new resin-glycosides, merremosides a, b, c, d, and e, from the tuber of Merremia mammosa (Convolvulaceae) [J]. *Chem Pharm Bull (Tokyo)*, 1996, **44**(9): 1680-1692.
[43] Yang M, Wang CC, Wang WL, *et al*. *Saposhnikovia divaricata*-an ethnopharmacological, phytochemical and pharmacological review [J]. *Chin J Integr Med*, 2020, **26**(11): 873-880.
[44] Xu L, Cai J, Tian A, *et al*. The effect of prim-*O*-glucosylcimifugin on tryptase-induced intestinal barrier dysfunction in Caco-2 cells [J]. *Biol Pharm Bull*, 2018, **41**(9): 1355-1361.
[45] Cao XY, Ni JH, Wang X, *et al*. Total glucosides of Paeony restores intestinal barrier function through inhibiting Lyn/Snail signaling pathway in colitis mice [J]. *Phytomedicine*, 2021, **87**: 153590.
[46] Wu XX, Huang XL, Chen RR, *et al*. Paeoniflorin prevents intestinal barrier disruption and inhibits Lipopolysaccharide (LPS)-induced inflammation in Caco-2 Cell monolayers [J]. *Inflammation*, 2019, **42**(6): 2215-2225.
[47] Qiu F, Zhong X, Mao Q, *et al*. The antidepressant-like effects of paeoniflorin in mouse models [J]. *Exp Ther Med*, 2013, **5**(4): 1113-1116.
[48] He X, Xing D, Ding Y, *et al*. Determination of paeoniflorin in rat hippocampus by high-performance liquid chromatography after intravenous administration of *Paeoniae* Radix extract [J]. *J Chromatogr B*, 2004, **802**(2): 277-281.
[49] Tjong Y, Ip S, Lao L, *et al*. Analgesic effect of *Coptis chinensis* rhizomes (Coptidis Rhizoma) extract on rat model of irritable bowel syndrome [J]. *J Ethnopharmacol*, 2011, **135**(3): 754-761.
[50] He K, Hu Y, Ma H, *et al*. Rhizoma *Coptidis* alkaloids alleviate hyperlipidemia in B6 mice by modulating gut microbiota and bile acid pathways [J]. *Biochim Biophys Acta*, 2016, **1862**(9): 1696-1709.
[51] Donnapee S, Li J, Yang X, *et al*. *Cuscuta chinensis* Lam: a systematic review on ethnopharmacology, phytochemistry and pharmacology of an important traditional herbal medicine [J]. *J Ethnopharmacol*, 2014, **157**: 292-308.
[52] Espley RV, Butts CA, Laing WA, *et al*. Dietary flavonoids from modified apple reduce inflammation markers and modulate gut microbiota in mice [J]. *J Nutr*, 2013, **144**(2): 146-154.
[53] Zhang R, Zhu X, Bai H, *et al*. Network pharmacology databases for Traditional Chinese Medicine: review and assessment [J]. *Front Pharmacol*, 2019, **10**: 123.
[54] Schulze-Osthoff K, Bantel H. Macrophage p38 kinase inhibition for liver regeneration [J]. *FEBS J*, 2017, **284**(24): 4196-4199.
[55] Korbecki J, Bajdak-Rusinek K. The effect of palmitic acid on inflammatory response in macrophages: an overview of molecular mechanisms [J]. *Inflamm Res*, 2019, **68**(11): 915-932.
[56] Li X, Li F, Zhang X, *et al*. Caspase-8 auto-cleavage regulates programmed cell death and collaborates with RIPK3/MLKL to prevent lymphopenia [J]. *Cell Death Differ*, 2022, **29**(8): 1500-1512.
[57] Song R, Li Y, Hao W, *et al*. Identification and analysis of key genes associated with ulcerative colitis based on DNA microarray data [J]. *Medicine (Baltimore)*, 2018, **97**(21): e10658.
[58] Sun CN, Wang FY, Li SX, *et al*. The influence of "Shao Yao Tang" to signal pathway expression of TLR2, PIK3CA, and AKT in colon tissues of UC rat models [J]. *Jiangsu J Tradit Chin Med*, 2019, **51**(11): 83-86.

Cite this article as: YANG Fengge, ZHANG Sihao, TIAN Danmei, ZHOU Guirong, TANG Xiyang, MIAO Xinglong, HE Yi, YAO Xinsheng, TANG Jinshan. Deciphering chemical and metabolite profiling of Chang-Kang-Fang by UPLC-Q-TOF-MS/MS and its potential active components identification [J]. *Chin J Nat Med*, 2023, **21**(6): 459-480.